Research Square

Preprints are preliminary reports that have not undergone peer review.
They should not be considered conclusive, used to inform clinical practice,
or referenced by the media as validated information.

Tetramerization of PKM2 alleviates traumatic brain injury by ameliorating mitochondrial damage in microglia

Haiyan Zhu
Nanjing Medical University
Huiwen Zhang
Nanjing Medical University
Xiao-Jing Zhao
The Affiliated Jiangning Hospital of Nanjing Medical University
Lingyuan Zhang
Nanjing Medical University
Xue Liu
Nanjing Medical University
Zhi-Yuan Zhang
Nanjing Medical University
Yi-Zhi Ren (ryz@njmu.edu.cn)
The Second Affiliated Hospital of Nanjing Medical University
Yong Feng
Jiangsu Cancer Hospital & Jiangsu Institute of Cancer Research & The Affiliated Cancer Hospital of Nanjing Medical University, Nanjing Medical University

Research Article

Keywords: PKM2, TBI, Microglia, Mitochondria, MFN2

Posted Date: September 6th, 2023

DOI: https://doi.org/10.21203/rs.3.rs-3279754/v1

License: This work is licensed under a Creative Commons Attribution 4.0 International License.
Read Full License

Abstract

Background

Traumatic brain injury (TBI) is a leading cause of death and disability worldwide. Microglial activation and neuroinflammation are key cellular events that determine the outcome of TBI, especially neuronal and cognitive function. Studies have suggested that the metabolic characteristics of microglia dictate their inflammatory response. The pyruvate kinase isoform M2 (PKM2), a key glycolytic enzyme, is involved in the regulation of various cellular metabolic processes, including mitochondrial metabolism. This suggests that PKM2 may also participate in the regulation of microglial activation during TBI. Therefore, the present study aimed to evaluate the role of PKM2 in regulating microglial activation and neuroinflammation and its effects on cognitive function following TBI.

Methods

A controlled cortical impact (CCI) mouse model and inflammation-induced primary mouse microglial cells in vitro were used to investigate the potential effects of PKM2 inhibition and regulation.

Results

PKM2 was significantly increased during the acute and subacute phases of TBI and was predominantly detected in microglia rather than in neurons. PKM2 inhibition by TEPP46 and shikonin inhibited microglial M1-like activation and attenuated neuroinflammation following TBI. The effects of general inhibition and tetramerization of PKM2 on microglial activation were compared, and we confirmed that the nuclear translocation of PKM2 is required for the generation of the pro-inflammatory microglial M1 phenotype. PKM2 tetramerization effectively transitioned microglial activation to an anti-inflammatory phenotype and maintained normal mitochondrial morphology by enhancing the interaction between PKM2 and mitofusin 2 (MFN2) in pro-inflammatory activated microglia. General inhibition and tetramerization of PKM2 attenuated cognitive function caused by TBI, whereas PKM2 tetramerization exhibited a better treatment effect.

Conclusion

Our experiments demonstrated the non-metabolic role of PKM2 in the regulation of microglial activation following TBI. Tetramerization or suppression of PKM2 can prevent the pro-inflammatory M1 microglia phenotype and improve cognitive function after TBI.

Introduction

Traumatic brain injury (TBI) is a significant cause of death and disability and can affect people of all ages(Collaborators, 2019). Cognitive impairment is one of the most common and destructive sequelae of TBI. Mitigating brain damage and promoting neural functional recovery following TBI can alleviate the burden on patients and society(Maas et al., 2017). However, owing to the complex pathophysiological processes of TBI, a comprehensive understanding of this disorder is lacking. Therefore, the pathogenesis of cognitive impairment after TBI needs to be further elucidated and finding effective therapeutic interventions is important.

The pathological process of TBI can be divided into primary and secondary stages. The primary stage is caused by the initial injury directly to the neural tissue, and includes axonal damage and diffuse neurovascular injury(Maas et al., 2008). The secondary stage is triggered by the initial injury and includes excitotoxicity, mitochondrial dysfunction, and neuroinflammation(Anthonymuthu et al., 2016; Dorsett et al., 2017; Jassam et al., 2017). These factors exacerbate each other and contribute to extensive neuronal loss. Neuroinflammation is characterized by persistent microglial activation, which can be observed using positron emission tomography (PET) with radioligands specific for microglial markers(Okello et al., 2009; Best et al., 2019). Microglia function as danger surveillance cells and respond by upregulating the metabolic machinery that enables phagocytosis and the release of pro-inflammatory cytokines(Scott et al., 2021). Microglial activation has been characterized into pro-inflammatory (M1) and anti-inflammatory (M2) states(Kumar et al., 2020). M1 and M2 microglia are oversimplified in their respective inflammatory roles, and current research suggests that microglia develop mixed phenotypes according to each foreign material within the CNS(Bernier et al., 2020). Persistent activation is a pro-inflammatory state that causes damage and neuron loss, ultimately leading to cognitive impairment(Bernier et al., 2020). Therefore, targeting microglia is a promising strategy for treating TBI.

Mitochondria, a dynamic double membrane organelle regulating cell health, play an importangt role in regulating neuropathology, neurogeneration, and immune activation in TBI. Studies suggest that changes in the metabolic signature of microglia underlie their response to inflammation(Peruzzotti-Jametti et al., 2021). Microglia prefer oxidative phosphorylation (OXPHOS) in the repair state, but shift to glycolysis in the pro-inflammatory state, and mitochondrial respiration decreases in this scenario as well(Nagy et al., 2018). Mitochondria are important organelles that regulate microglial cell metabolism and activation state(Fairley et al., 2021). The available evidence suggests that rescuing mitochondria in TBI is a potential therapeutic approach(Ahluwalia et al., 2021). Recent studies have shown that mitochondrial impairment in microglia amplifies NLRP3 inflammasome pro-inflammatory signaling in cell cultures and animal models of Parkinson’s disease and cerebral ischemia/reperfusion injury(Sarkar et al., 2017; Gong et al., 2018). Additionally, blocking excessive mitochondrial fission normalizes mitochondrial respiration and attenuates chemokines(Nair et al., 2019). Mitochondria are dynamic organelles, and the balance between biogenesis, fission, fusion, and mitophagy maintains a healthy mitochondrial population(Pickles et al., 2018). Therefore, maintaining a balance between fission and fusion of mitochondria in microglia after TBI may be an effective pharmacological strategy.

The M2 isoform of pyruvate kinase (PKM2), a rate-limiting enzyme in glycolysis, exists as either a low-activity dimer or high-activity tetramer(Alquraishi et al., 2019). Under physiological conditions, approximately 30–35% of PKM2 is monomeric, and the remaining majority is the highly active tetrameric form; however, under ischemic or inflammatory conditions, dimeric PKM2 is stimulated. Compelling evidence has shown that dimeric PKM2 can translocate to the nucleus to interact with HIF-1α, leading to the production of pro-inflammatory cytokines and M1 macrophage polarization(Palsson-McDermott et al., 2015; Wang et al., 2017; Kong et al., 2019). Downregulation of PKM2-mediated glycolysis has been reported to exhibit anti-inflammatory effects in an *in vitro* model of cerebral ischemia(Gao et al., 2020). Moreover, tetrameric PKM2 opens the tricarboxylic acid cycle (TCA) and electron transport chain to consume excess reactive oxygen species (ROS) and protect mitochondria(Zhang et al., 2019). Apart from its canonical pyruvate kinase (PK) activity, recent studies have found that PKM2 participates in the modulation of mitochondrial fusion. In particular, PKM2 interacts with mitofusin 2 (MFN2), a key regulator of mitochondrial fusion, to improve mitochondrial qualification and regulate metabolism in cancer cells(Li et al., 2019). However, the effect of adjusting the ratio of PKM2 dimer to Tetramer status on mitochondrial qualification and microglia activation status is unclear. It also remains to be seen whether regulating the molecular conformation of PKM2 plays a role in pathological changes and cognitive impairment caused by TBI. In the present study, we found that tetramerization of PKM2 enhanced the interaction between PKM2 and MFN2, and improved the mitochondrial qualification of microglia. Tetramerization of PKM2 alleviates cognitive impairment following TBI by promoting microglial switching to anti-inflammatory and repair states.

Materials and Methods

2.1 Animals

C57/B6 mice (8-weeks-old) weighing 20–24 g, were obtained from the Experimental Animal Center of Nanjing Medical University. The mice were housed at a suitable temperature and humidity on a 12-h / 12-h light / dark cycle. All the mice had free access to food and water. In total, 118 healthy mice of either sex were used in this study. No specific statistical methods were performed for sample calculation and previous studies were used as a reference(Carneiro et al., 2018). Neurological Severity Score (mNSS) tests were performed on 118 C57/B6 mice (8 weeks old) weighing 20-24 g each. One mouse with an abnormal score was excluded from the experiment and replaced with one of the same sex. In the first part of this study, mice were divided into five groups (n = 14 animals/group): the sham group, the TBI 1d group, the TBI 3d group, the TBI 7d group and the TBI 14d group. In the second part of this study, mice were divided into four groups (n = 12 animals/group): the sham group, TBI+vehicle group, the TBI+SK group, the TBI+TEPP46 group. No randomization was performed to allocate subjects in the study. Behavioural experiments were performed between 2 and 5 p.m., and treated animals were assessed prior to control animals. During experiments and analysis, the investigators were blinded to experimental group. Animals were identified by earmarks that assigned numbers to each, which were announced to the

investigator only after finishing experiments and analysis. Animals were killed using cervical dislocation at the time of biochemical analysis.

All procedures were conducted in strict accordance with the ARRIVE Guidelines (Animal research: reporting of in vivo experiments) and approved by the Ethics Committee of Nanjing Medical University College and the National Institutes of Health Guide for the Care and Use of Laboratory Animals (#IACUC-2011010). The study was not pre-registered.

2.2 Experimental TBI model

A controlled cortical impact model was adopted to establish TBI groups based on previously published research(Ren et al., 2020). To ensure that there were no adverse effects on the physiological state of mice, 50mg/kg dose of pentobarbital were administered intraperitoneally for anesthesia. Each anesthetized mouse was placed on a stereotactic machine with its skull exposed. A portable drill and a 3.5 mm ring bit were used to perform a craniotomy in the right parietal temporal cortex, preserving the integrity of the dura. Then, a convex tip (diameter of 3 mm) was used to generate a 1.2 mm depression at a speed of 4.5 m/s causing mild damage. The bone flap was discarded and the scalp was sutured and closed. After each TBI or sham procedure, mice were immediately placed on a heating pad (37°C) for at least 15 minutes to maintain the body temperature. An air heater was also settled to keep the animals warm. Then the mice were allowed to settle in cages until they recovered from anesthesia. No analgesics were applied due to their potential to induce mitochondria dysfunction, which might interfere with the effects of the drugs we used in the experiment. Still, to ease the pain caused by the procedure, jelly was given to the mice to supplement energy and water. And after surgery, 0.15 mg/kg buprenorphine hydrochloride (Recktt Benckiser Healthcare Ltd., Kingston-upon-Thames, UK) was injected subcutaneously to each of mice to reduce pain after surgery. In addition, the same procedure, excluding the hit, was performed in the sham group. All mice regained consciousness within 1 h of surgery. Nine mice from TBI group died during recovery before tests and were excluded from the study.

2.3 Drug treatment

Shikonin was purchased from MedChemExpress Biochemical (Cat. No. No. HY-N0822, Shanghai, China 2021). TEPP46 was purchased from MedChemExpress Biochemical (Cat. No. No. HY-18657, Shanghai, China, 2021). Mice were continuously administered intraperitoneal injections of 5 (shikonin) or 50 mg/kg/day (TEPP46) 24 h after brain injury. The doses were selected based on the results of previous studies(Xie et al., 2016; Angiari et al., 2020). The sham and TBI groups received the same dose of drug solvent. Cells were treated *in vitro* with different concentrations for 30 min.

2.4 Cortical lesion volume

Cortical sections were obtained every 0.01 mm to determine lesion volume. Lesion volume was calculated from the summation of the defect areas on each tissue slice using ImageJ software (National Institutes of Health, Bethesda, MD, USA).

2.5 Behavioral tests

Behavioral tests were usually performed between 1 and 3 pm. Fear conditioning tests (FCTs) were used to evaluate memory and cognitive function in mice(Cibelli et al., 2010; Terrando et al., 2015). The experimental environment was a test box, and the bottom of the box was energized to establish an environment of fear using noise and electric shock. The experimental procedure included three stages: adaptation, training, and testing, which were completed at the same time point for three consecutive days. During the adaptation stage, the mice were placed in a box and allowed to adapt for 5 min without any stimulation. During the training phase, mice were subjected to 30 s (75 dB, 2.8 kHz) sound stimulation and then 2 s electric shock (1 mA) at the 3^{rd} and 5^{th} minutes, respectively. The entire process lasted 7 min. During the testing stage, there was only sound stimulation, and the participants' fear of the environment was evaluated by the percentage of freezing time (freezing). This test was conducted on the third, seventh, and 14^{th} day after TBI.

Morris water maze (MWM) test was performed to evaluate spatial learning and reference memory of mice. The device of MWM consisted of a circular pool with a diameter of 120 cm and height of 70 cm and a cylindrical platform with a diameter of 8cm. The pool was filled with opaque water maintained at 20 ± 1 °C and equally divided into four quadrants. The platform was placed in the center of one of the quadrants. During the initial 5 days, mice were trained to found the hidden platform when started from random locations around the pool. The escape latency of the mice was recorded by TopScan Realtime Option system and analyzed in 5-day training session. On sixth day, the platform was removed and the probe test was conducted. The mice was allowed to freely explore the pool for 60s and the number of mice crossing the platform was recorded and analysed.

2.6 Immunohistochemistry and hematoxylin-eosin staining (HE)

All animals that underwent behavioral tests were anesthetized with 4% isoflurane and perfused through the heart with 4% paraformaldehyde. The brain tissue was fixed with 4% paraformaldehyde for 24 h and then embedded in paraffin. Subsequently, the specimens were cut into 10 μm-thick sections. The sections were dewaxed in xylene, rehydrated using decreasing concentrations of ethanol, and washed in phosphate-buffered saline (PBS). The sections were stained with hematoxylin and eosin (HE).

2.7 Immunofluorescence and Confocal Microscopy

All animals that underwent behavioral tests were anesthetized with 4% isoflurane and perfused through the heart with 4% paraformaldehyde. Brain tissue was fixed with 4% paraformaldehyde for 24 h, followed by 30% sucrose solution for continuous dehydration at 4 °C for three days. Sucrose solution was replaced every 24 h to ensure that the brain tissue was fully dehydrated. The tissue was then embedded with optimal cutting temperature (OCT) compound and cut into 10-um-thick sections using a frozen sectioning machine (Leica, CM1860). The sections were incubated overnight at 4 °C with NeuN (RRID:AB_2532109, 1:300, Abcam), Iba1 (RRID:AB_2832244, 1:200, Abcam), and GFAP (RRID:AB_561049, 1:300; Cell Signaling Technology). Sections were washed and incubated with the following secondary antibodies: donkey anti-rabbit IgG (RRID: AB_2535792, 1:1000, Thermo) and donkey anti-mouse IgG (RRID: AB_2732856, 1:200, Abcam) for 1 h at room temperature, and then washed four times with PBS. Cell nuclei were stained with 4’,6-diamidino-2-phenylindole (DAPI, Southern Biotech, Cat. No. 0100–20, 2020). Finally, each section was imaged using a confocal microscope (Zeiss, LSM800). Images were analyzed using ImageJ software.

2.8 Terminal deoxynucleotidyl transferase dUTP nick end labeling (TUNEL) Staining

The level of apoptosis in mouse neurons was detected using the TUNEL Bright Green Apoptosis Detection Kit (Vazyme, Cat. No. A112-01, 2020). The brain tissue sections were fixed in 4% paraformaldehyde (prepared in PBS) for 30 min at room temperature. The sections were washed four 4 times with PBS, incubated with 0.2% Triton-X100 for 10 min, and then incubated with 1% BSA for 1 h at room temperature. Following this, an equilibration solution (100 μL of 1 × equilibration buffer) was added to each sample to equilibrate for 20 min, and then 50 μL working solution (ddH2O, 5 × equilibration buffer, recombinant TdT enzyme) was added for 1 h at 37 °C. Sections were washed four 4 times with PBS, incubated overnight at 4 °C with neuronal antibodies (RRID:AB_2532109, 1:300, Abcam), and then incubated with donkey anti-mouse IgG(RRID:AB_2732856, 1:200, Abcam) secondary antibodies. All sections were imaged using a confocal microscope (Zeiss, LSM800). Images were analyzed using ImageJ software.

2.9 Brdu labeling

Bromodeoxyuridine (BrdU), a nucleoside analog that commonly used to detect proliferating cells, was applied to evaluate neurogenesis after TBI. BrdU (50mg/kg, Cat. No. HY-15910) was intraperitoneally injected to mice twice a day at 6h interval for 14 consecutive days before euthanized. The brain of mice was harvested for immunofluorescence assays.

2.10 Western blot analysis

Mice were sacrificed by cervical dislocation and the edema zone around the injured cortex of the brain was collected. RIPA Lysis buffer (Beyotime, Cat. No. P0013B, 2021) 200 μL containing 1 μM PMSF was added to each sample, and subsequently homogenized at 12000 × g for 20 min at 4 °C. After centrifugation, the supernatant was collected into a new tube. BCA kit (Beyotime, Cat. No. P0012, 2021) was used to normalize the amount of protein at 40 μg per lane. Equal amounts of protein were separated by 8–15% sodium dodecyl sulfate-polyacrylamide gel electrophoresis and then transferred to a polyvinylidene difluoride membrane. Following this, the membranes were blocked for 2 h in 5% non-fat dry milk (NFDM) and incubated with the following primary antibodies: NLRP3 (RRID:AB_2490202, 1:1000, AdipoGen), ASC (1:1000, Abcam, ab283684), Caspase1 (RRID:AB_2889889, 1:1000, Abcam), IL-1β (RRID:AB_2715503, 1:1000, CST), PKM2 (RRID:AB_1904096, 1:1000, CST), p-PKM2 (RRID:AB_1950369, 1:1000, CST), MFN2 (RRID:AB_2266320, 1:1000, Proteintech), β-actin (RRID:AB_2797445, 1:10000, Bioworld), and lamin B1(RRID:AB_443298, 1:1000, Abcam) overnight at 4 °C. The next day, the membranes were washed three times with TBS-T(TBS + 0.1% Tween-20) for 10 min, probed with an HRP-linked secondary antibody for 1 h at room temperature, and washed three times with TBS-T. The membranes were then incubated with enhanced chemiluminescence (ECL) (Sparkjade, Cat. No. ED0015-C, 2020), and visualized using the Tanon-5200Multi system (17T15NBFLI6-953). The raw density of the bands was analyzed using image J software. All values were normalized to those of β-actin and lamin B1.

2.11 Quantitative RT-PCR

Total RNA was extracted using TRIzol reagent (Invitrogen, Cat. No. 15596018, 2020), according to the manufacturer's protocol. Next, 1 μg of total RNA was used to synthesize cDNA using a cDNA synthesis kit (Vazyme, Cat. No. R223-01, 2020). All PCRs were performed on a Light Cycler 96 thermocycler (Roche). Primer sequences for the target genes are listed in Table 1. Melting curve analysis was performed to confirm the specific PCR products of interest. Relative gene expression was calculated using the ΔΔCt method and normalized to β-actin expression.

2.12 Transmission electron microscopy (TEM)

The animals were anesthetized with 4% isoflurane and perfused through the heart with 4% paraformaldehyde. The edema zone around the injured cortex of the brain was collected, cut into 2–3 mm pieces, and soaked in glutaraldehyde solution for seven days at 4 °C. After fixation, all samples were washed three times for 15 min and then fixed with 0.1% osmium acid at 25 °C for 2 h. All samples were dehydrated with a concentration gradient ethanol solution (50, 70, 80, 90, and 95%) for 15 min and treated with pure acetone for 20 min. Following this, samples were gradient infiltrated with an embedding agent, heated, and polymerized, trimmed, sectioned (50 nm) with an ultrathin microtome, stained with uranyl acetate 50% ethanol saturated solution for 1 h, and rinsed with ddH_2O. Representative areas were

chosen to generate ultrathin sections, which were viewed using a transmission electron microscopy (TEM) system at an accelerating voltage of 80 kV.

2.13 Cell extraction

Primary microglia were obtained from one- to three-day-old mice pups. In total, fifty mice pups were sterilized in alcohol and killed by cutting both carotid arteries without decapitating the head, then the cerebral cortex were carefully removed, and placed in serum-free F12 medium (Wisent, Cat. No. 319-075-CL, 2020). The brains membranes were peeled off with micro tweezers under a visual microscope. Following this, microscissors were used to cut the cortical tissue into approximately 1 mm × 1 mm sections. Three to four cerebral cortices were mixed 5 mL 0.25% pancreatin and DNase were added to the medium, and the tissue was placed in a 37 °C incubator for 20 min. After digestion, 2 mL of serum was added, and the mixture was transferred to a 50 mL centrifuge tube. The suspension was sieved twice with a 200-mesh cell sieve, transferred to a T75 cell culture flask, and then placed in a 37 °C cell incubator. After 7–10 days, the culture medium was collected to obtain the primary microglia.

2.14 Cell culture

Primary microglial cells were cultured in T75 cell culture flasks in F12/DMEM (Wisent, Cat. No. 319-075-CL, 2020) containing 10% fetal bovine serum (Gibco, Cat. No. 10099141C, 2020), 100 U/mL penicillin, and 0.1 mg/mL streptomycin. Mouse neuro-2a neuroblastoma cells were cultured in T75 cell culture flasks in DMEM (Wisent, Cat. No. 319-005-CL, 2020) containing 10% FBS (Gibco, Cat. No. 10099141C, 2020), penicillin (100 U/mL), and streptomycin (100 μg/mL). After the cell density reached approximately 90%, cells were passaged and plated. The specific steps were as follows: washing twice with PBS, adding 5 mL of 0.25% pancreatin, incubation at 37 °C for 5 min, adding the culture medium, transferring the cell suspension into a 15 mL centrifuge tube, centrifuging at 1000 rpm for 5 min, resuspending the cells in fresh medium, and counting the cells. The 12-well plate was plated at 1×10^5 cells/well, the 6-well plate was plated at a density of 1×10^6 cells/well, and the cells were passaged at a ratio of 1:3. Mouse Neuro-2a neuroblastoma cells (ATCC® CCL-131TM, RRID: CVCL0470) (the cell line is not listed as a commonly misidentified cell line by the International Cell Line Authentication Committee) were grown in ATCC-formulated Eagle's minimal essential medium (ATCC®, Cat. No. 30–2003, 2019). The maximum number of passages for Neuro-2a was 15.

2.15 Cell Transfection

Primary microglia were seeded into 12-well plates at a density of 6×10^4 cells/well after trypsinization and passage. Cell transfection was conducted after cell growth was stabilized using lipofectamine reagent (Thermo Fisher Scientific, Cat. No. STEM00015, 2021), according to the manufacturer’s

instructions. Small interfering RNA (siRNA) was synthesized by the GenePharma Biological Company (Gene Pharma, China).

2.16 Cell processing

Primary microglia were divided into control, LPS (1 μg/mL), LPS+Shikonin (1 μM), LPS+Shikonin (5 μM), and LPS+Shikonin (10 μM) groups. The LPS group was stimulated with LPS for 12 h and the LPS + SK group was incubated with different concentrations of shikonin for 30 min after 12 h of LPS stimulation. After treatment, cells were harvested for subsequent experiments.

2.17 Cell Counting Kit-8 (CCK-8) assay

A CCK-8 cell counting kit (Vazyme, Cat. No. A311-01, 2021) was used to detect the cell viability of primary microglia treated with different concentrations of drugs to determine the degree of drug toxicity. Primary microglia were seeded in 96-well plates. After the cells attached, they were grouped and treated with a concentration gradient of shikonin (1, 5, 10, or 20 μM). After 30 min of treatment, 10 μL of CCK-8 solution was added and the samples were incubated in the dark for 2 h at 37 °C. Absorbance was measured at 450 nm using a microplate reader.

2.18 Annexin V-FITC/PI apoptosis detection

Apoptosis of neuronal N2A cells was detected using an Annexin V-APC/PI apoptosis analysis kit (Absin, Cat. No. abs50009, 2021). First, primary microglia and Neuro-2a neuroblastoma cells were seeded on a 12-well plate, and the microglia were grouped into control, LPS (1 μg/mL), and LPS + shikonin (5 μM) groups. Samples were treated with LPS for 12 h and shikonin for 30 min, the medium was discarded, fresh medium was added, the medium was collected after 12 h, and N2A cells were added to conditionally culture N2A cells for 12 h. After the conditioned culture was complete, the cells were washed twice with PBS, and 1 mL of trypsin was added to each well and incubated for 3 min to detach. Cells were collected in a flow tube and centrifuged at 1000 rpm for 5 min, the supernatant was discarded, and the pellet was washed twice with PBS. Then, 100 μL of 1 × binding buffer was added and the individual samples were mixed by pipetting, and 5 μL of Annexin V-FITC and 5 μL PI Staining Solution were added in the dark. The cells were then incubated for 10 min at room temperature. The cells were analyzed using a FACSCalibur flow cytometer, and the final data were processed using FlowJo flow cytometry analysis software.

2.19 Mito-Tracker Red assay

The morphology of cell mitochondria was observed by labeling mitochondria with MitoTracker Red (AAT Bioquest, Cat. No. 22698, 2020). Microglia were seeded in a confocal dish. After the cells were attached,

LPS (12 h) and LPS+Shikonin (30 min) stimulations were performed. The samples were washed twice with PBS, 10 μM MitoTracker Red was added, and the cells were incubated for 20 min. Following this, the cells were added to a medium containing 1 μM Hoechst, incubated for 1 min in the dark, and mitochondrial morphology was observed under a laser confocal microscope (ZEISS, LSM800).

2.20 Mitochondrial membrane potential (MTΔΨ)

A mitochondrial membrane potential detection kit (JC-1) (Beyotime, Cat. No. C2006, 2021) was used to detect mitochondrial membrane potential. First, the cells were seeded into a 12-well plate and divided into the control, LPS (1 μg/mL), and LPS+Shikonin (5 μM) groups. The samples were treated with LPS for 12 h and shikonin for 30 min, collected in a flow tube, and centrifuged at 1000 rpm for 5 min. Next, 1 mL of JC-1 staining working solution was added and the cells were incubated for 20 min. After incubation, the cells were washed twice with 1 × JC-1 staining buffer and 500 μL of 1 × JC-1 staining buffer was added. Finally, the mitochondrial membrane potential was determined using a FACSCalibur flow cytometer, and the final data were processed using the FlowJo flow cytometry analysis software.

2.21 PKM2 nuclear translocation by immunofluorescence staining

Microglia were seeded into a 12-well plate and then divided into control, LPS (1 μg/mL), and LPS+Shikonin (5 μM) groups. The cells were fixed with 4% paraformaldehyde for 15 min. After washing with PBS, cell membranes were lysed with 0.5% Triton for 20 min at room temperature. The cells were blocked with PBST containing 1% BSA for 30 min. Then, the cells were incubated with PKM2 antibodies (RRID: AB_1904096, 1:200, CST) at 4 °C overnight. and The next day, after washing, the cells were incubated with the corresponding fluorescent secondary antibody (RRID:AB_2722623, 1:200, Abcam) for 1 h at room temperature. Finally, 4 -6-Diamidino-2-phenylindole (DAPI; Southern Biotech, Cat. No. 0100–20, 2020) was added to each plate, and the protein expression of PKM2 was observed using an inverted fluorescent microscope (OLYMPUS).

2.22 Co-immunoprecipitation (Co-IP)

BV2 cells were seeded into 12-well plates. Cells were lysed using 200 μL of immunoprecipitation lysis buffer and 10 μL of the lysates were collected as input samples. PKM2 antibody (RRID: AB_1904096, 1:100, CST) was added to the remaining lysates and incubated at 4 ℃ overnight. Subsequently, 20 μL Protein A/G magnetic beads (MCE, Cat. No. HY-K0202, 2021) were added at 4 ℃ for 2 h. After washing and boiling, immunoprecipitates were separated by SDS-PAGE and probed with an MFN2 antibody (RRID: AB_2266320, 1:300, Proteintech).

2.23 Statistical Analysis

GraphPad Prism 8 software was used for all statistical analyses. The Shapiro-Wilk test was used to determine that the data were normally distributed. Two-way analysis of variance was used to compare two groups in multiple groups, and the Bonferroni method was used to compare the differences between the two groups. The results were presented as mean ± SD of ≥ 3 independent biological replicates. Significant differences were defined as $P < 0.05$.

Results

3.1 PKM2 expression increased with neuroinflammation

A controlled cortical impact (CCI) animal model to mimic moderate TBI was based on our previous study(Ren et al., 2020). Cerebral blood flow images revealed significant tissue defects and disturbances in blood flow (Fig. 1A). Contextual FCT was performed to evaluate cognitive function after TBI. FCT was performed at three, seven- and 14-days post-injury and showed that learning and memory functions were severely impaired at three days post-injury (Fig. 1B–C). ELISA was used to detect the pro-inflammatory cytokines IL-1β, IL-6 and TNF-α in the peri-contusional cortex and plasma from one to fourteen post-TBI (Fig. 1D–F). These pro-inflammatory cytokines significantly increased at one-day post-injury and maintained a high level until seven days post-injury. Additionally, immunofluorescent staining of the microglia/macrophage marker Iba1 showed that a large number of microglia were activated until seven days post-injury (Fig. 1H–I). The increase in pro-inflammatory cytokines in the plasma was delayed compared with that in the peri-contusional cortex (Fig. S1A-C). And iNOS also observed significantly increased following TBI in both peri-contusional cortex (Fig. 1G) and plasma (Fig. S1D). These results are consistent with those of previous studies(Jassam et al., 2017). PKM2, a key glycolytic enzyme, participates in central and peripheral inflammation(Xie et al., 2016; Gao et al., 2020). To determine whether PKM2 was involved in TBI-induced inflammation, we investigated the protein expression profiles of PKM2 in the peri-contusion cortex at different time points. We found that the expression of PKM2 dramatically increased at three- and seven-days post-injury (Fig. 1J–K), which was similar to Iba1 expression (Fig. 1H–I). Moreover, data from immunoreactivity detected by confocal microscopy at seven days post-injury revealed that PKM2 was predominantly expressed in microglia, but not in neurons (Fig. 1L–M). This result is in line with a previous RNA-sequencing study showing that neurons and glial cells express distinct splicing isoforms of the Pkm gene, namely, Pkm1 and Pkm2, respectively(Zhang et al., 2014). These results indicate that PKM2 is involved in microglial activation and neuroinflammation following TBI.

3.2 PKM2 inhibition and tetramerization

The effect of targeting PKM2 in microglia was further evaluated based on variations in activated states. Three methods for targeting PKM2 were chosen as described in previous studies(Zhang et al., 2017; Blum

et al., 2021). First, we used three PKM2-specific siRNAs (siPKM2(1), siPKM2(2), and siPKM2(3)). Second, shikonin, the main component of the traditional Chinese medicine community, has been widely used as a PKM2 general inhibitor and significantly inhibits PKM2 canonical activity and glycolysis(Xie et al., 2016). Third, TEPP-46, a small molecule used as a PKM2 activator, selectively increased canonical PKM2 activity and decreased noncanonical activity(Blum et al., 2021). LPS-induced primary microglia were cultured, and RT-PCR and western blotting confirmed that siPKM2(1) and siPKM2(2) effectively knocked down PKM2 expression (Fig. S2A–B). Primary microglia were cultured and activated, and according to the RT-PCR assay, pro-inflammatory cytokines, including IL-1β, IL-6, and TNF-α, were significantly reduced by siPKM2 (Fig. S2C–E). We further validated the effect of shikonin and TEPP-46 on the balance between dimers and tetramers. Disuccinimidyl suberate (DSS)-linking data demonstrated that shikonin significantly reduced the expression levels of both PKM2 dimers and tetramers, whereas TEPP-46 treatment resulted in a significant increase in tetrameric PKM2 in primary microglia (Fig. 2A–B). Cell proliferation was detected using the CCK8 kit, and the data showed that shikonin reduced cell viability at a higher concentration (30 μM). In contrast, TEPP-46 did not exhibit cytotoxicity at high concentrations (Fig. S2F–G). Shikonin and TEPP-46 significantly reduced the increase in pro-inflammatory cytokines, including IL-1β, IL-6, and TNF-α, in activated microglia (Fig. 2C–E and H–J). Shikonin did not affect anti-inflammatory cytokines, including IL-10 and CD206, whereas TEPP-46 further elevated the expression of IL-10 and CD206 in pro-inflammatory activated microglia (Fig. 2F–G, K–L). These results indicate that modulation of the balance between dimers and tetramers leads to differential microglial activation, and tetramerization of PKM2 transitions microglial activation into an anti-inflammatory phenotype.

3.3 Tetramerization and increased intracytoplasmic PKM2

The effects of shikonin and TEPP-46 on microglial activation were further investigated. It has been reported that PKM2 forms tetramers in the cytoplasm and cannot enter the nucleus only when dimeric PKM2 forms a complex in which PKM2 enters the nucleus(Yang et al., 2012). Therefore, we evaluated the subcellular localization of PKM2 following treatment with shikonin and TEPP-46. Western blot analysis showed that shikonin significantly reduced the expression level of PKM2 in the nucleus but did not affect PKM2 expression in the cytoplasm of pro-inflammatory activated microglia (Fig. 3A–B). The expression level of PKM2 in the cytoplasm significantly increased and intranuclear PKM2 significantly decreased after TEPP-46 treatment (Fig. 3C–D). These results were confirmed by immunofluorescence staining of PKM2. Both TEPP-46 and shikonin significantly reduced intranuclear PKM2 levels, but only TEPP-46 showed a slight increase in intracytoplasmic PKM2 levels (Fig. 3E–F). Additionally, phosphorylation of PKM2 at tyrosine-105 (Y-105), which has been reported to enhance PKM2 nuclear accumulation, was examined(Alquraishi et al., 2019). Western blotting analysis showed that the expression of p-PKM2 (Y-105) was significantly reduced by TEPP-46 and shikonin (Fig. 3G–H). These results confirmed that both shikonin and TEPP-46 blocked PKM2 nuclear translocation, but only TEPP-46 significantly increased the intracytoplasmic PKM2 levels in pro-inflammatory activated microglia.

3.4 Tetramerization of PKM2 ameliorated mitochondrial damage

The intracytoplasmic PKM2 tetramer is suspected to be increased by TEPP-46, as the major distinction between shikonin and TEPP-46 may be the transition of microglial activation to an anti-inflammatory phenotype. The PKM2 tetramer opens the TCA cycle and drives cell metabolic alterations to protect the mitochondria from drug attack(Zhang et al., 2019). Accumulating evidence suggests that the PKM2 tetramer enhances PK activity and regulates mitochondrial function by increasing translocation into the mitochondria under inflammatory conditions(Yi et al., 2020; Li et al., 2022). Therefore, we evaluated the effects of shikonin and TEPP-46 on mitochondrial morphology and membrane potential in pro-inflammatory microglia. Under physiological conditions, normal mitochondria exhibit a long and tubular morphology. However, under inflammatory conditions, damaged mitochondria exhibit punctate morphology. MitoTracker Red staining revealed that TEPP-46 could significantly maintain normal tubular mitochondrial morphology in pro-inflammatory activated microglia, whereas in the shikonin-treated group, most mitochondria exhibited punctate morphology (Fig. 4A). The above evidence indicates that PKM2 tetramerization may maintain mitochondrial morphology through a certain mechanism. Additionally, the effect of TEPP-46 on microglial mitochondrial protection was further confirmed by the mitochondrial membrane potential test based on JC-1 staining. Our results showed that TEPP-46 also improved the mitochondrial membrane potential depletion induced by LPS in microglia, but this deficit was not restored by shikonin treatment (Fig. 4B–C). These results suggest that differences in microglial activation between shikonin and TEPP-46 may be caused by PKM2 tetramerization.

3.5 Tetramerization of PKM2 by TEPP46 protect mitochondria in microglia via enhancing the interaction of PKM2 with MFN2

The underlying mechanism by which PKM2 exerts its protective effect on mitochondrial morphology in microglia was investigated. Mitochondrial morphology is predominantly determined by three factors: mitochondrial fusion, fission, and mitophagy(Mishra and Chan, 2014). PKM2 protects mitochondria from over-fragmentation by interacting with MFN2, which plays an important role in promoting mitochondrial fusion(Li et al., 2019). We determined whether increased cytoplasmic PKM2 was involved in the interaction between MFN2 and mitochondrial fusion. Co-IP showed an interaction between endogenous PKM2 and MFN2 in pro-inflammatory activated microglia in response to TEPP-46 and shikonin treatment. Co-IP analysis showed that TEPP-46 significantly enhanced the interaction between PKM2 and MFN2 in pro-inflammatory activated microglia, according to the relative quantification of MFN2 increasing with PKM2 following TEPP-46 treatment, whereas shikonin did not exhibit the same effect (Fig. 5A–B). These results suggest that the enhanced interaction between PKM2 and MFN2, resulting from TEPP-46, may be involved in microglial mitochondrial protection and activation.

To confirm the above assumption, we designed three MFN2-specific siRNAs (siMFN2 (1), siMFN2 (2), and siMFN2 (3)), and RT-PCR and western blotting results confirmed that siMFN2 (1) and siMFN2 (2) effectively knocked down MFN2 expression (Fig. 5C–E). Knockdown of MFN2 in pro-inflammatory activated microglia significantly affected inflammatory cytokine gene expression, which blunted the effect of TEPP-46 in decreasing the expression of TNF-α, IL-6, and IL-1β (Fig. 5F–H). There was an increase in the levels of anti-inflammatory cytokines including CD206 and IL-10 (Fig. 5I–J). Additionally, the JC-1 staining test showed that the effect of TEPP-46 on maintaining the mitochondrial membrane potential was blunted by siMFN2 (Fig. 5K–L). These results indicated that the enhanced interaction between PKM2 and MFN2 may play an important role in mitochondrial protection.

3.6 Tetramerization of PKM2 in microglia alleviate cognitive impairment

The neuroprotective effects were further investigated, especially with regard to neuronal survival and cognitive preservation following TBI. Schematics of the brain injury caused by the CCI animal model and the mode of administration are presented in Fig. 6A. The detection timeline is shown in Fig. 6B. The administration of vehicle or shikonin (5 mg/kg, i.p.) and TEPP-46 (50 mg/kg, i.p.) to control the cortical impact was performed each day after injury. FCT was assessed at three-, seven-and fourteen-day-post injury. When analyzing three-and fourteen-day-post injury, shikonin and TEPP-46 treatments significantly increased the percentage of freezing behaviors compared to vehicle-treated TBI mice (Fig. 6C–D). Fourteen days post injury, TEPP-46 treatment exhibited a better ameliorative effect than shikonin treatment. Moreover, morris water maze test was employed to measure spatial memory. The results also showed that TEPP-46 had a better therapeutic effect (Fig. 6E–F). We then examined Iba1 by immunofluorescence analysis and confocal microscopy, and the images showed that microglia presented as a ramified form with elongated and thin cellular structures in the sham group, in the TBI group, microglia presented as the amoeboid form with a distended cell body (Fig. S3A-B). In the shikonin and TEPP-46 treated group, microglia presented a cell morphology between the ramified and amoeboid forms, and the immunofluorescence intensity was also significantly decreased. These results further confirmed that shikonin and TEPP-46 induced microglial activation to present different phenotypes. Moreover, HE staining showed that shikonin and TEPP-46 treatments significantly limited trauma size following TBI. Importantly, TEPP-46 treatment showed a better repair capability and significantly reduced lymphocytic infiltration (Fig. 6G–H).

Neurogenesis and neurons survival are strongly associated with post-TBI recovery. Both shikonin and TEPP-46 treatment increased BrdU labeled neurons and reduced TUNUL-positive neurons following TBI, but more neurons were regenerated and preserved by TEPP-46 treatment compared to the shikonin group (Fig. 7A–D). Taken together, the inhibition of total PKM2 in microglia by shikonin or the induction of tetramerization of PKM2 by TEEP-46 could increase neurogenesis and ameliorate neuronal loss following TBI. In vitro, the effect of PKM2 tetramerization in microglia on the survival rate of neurons was further evaluated by collecting conditioned media from activated BV2 microglia induced by LPS (1 μM) for 12 h

and treated with shikonin for 30 min or TEPP-46 for 12 h (Fig. 7E). The conditioned media were added to N2a cells for 12 h, and N2a cells were stained with PI (Annexin-FITC/PI) for flow cytometry analysis. The results demonstrated that compared to the LPS group, microglia treated with both TEPP-46 (10 μM) and shikonin (10 μM) reduced inflammation-induced neuronal loss. However, TEPP-46 reused more neurons under inflammatory conditions (Fig. 7F–G). These findings suggest that conditioned media collected from TEPP-46- and shikonin-treated microglia could significantly reduce inflammation-induced neuronal loss, and that the effect of TEPP-46 was significantly superior to that of shikonin. In addition to suppressing pro-inflammatory cytokines, TEPP-46 further elevated the expression of anti-inflammatory cytokines, including IL-10 and CD206, in pro-inflammatory activated microglia. Both shikonin and TEPP-46 blocked PKM2 nuclear translocation (Fig. 3–5); however, TEPP-46 significantly increased intracytoplasmic PKM2 and protected mitochondria by enhancing its interaction with MFN2 in pro-inflammatory activated microglia. Collectively, these data indicate that decreasing intranuclear PKM2 levels can protect neurons from inflammation-induced damage. Moreover, increasing intracytoplasmic PKM2 levels may have beneficial effects on neuronal survival.TEM was used to observe mitochondrial morphology in microglia following TBI. The ultrastructure of normal mitochondrial morphology is characterized by a smooth outer membrane and an inner membrane that is contiguous with a vesicular type of cristae. The morphology of damaged mitochondria is characterized by a swollen appearance with damaged or lost cristae and a dark matrix(Chao et al., 2019). We found that TEPP-46 could maintain mitochondrial morphology to a great extent following TBI (Fig. 7H). These results above demonstrated that tetramerization of PKM2 by TEEP-46 exhibited a better treatment effect, indicating that protection of mitochondrial qualification following TBI, by enhancing the interaction of PKM2 with MFN2, contributed to increased treatment efficiency.

Discussion

In this study, we investigated the mechanisms underlying the regulatory effects of a key glycolytic enzyme, PKM2, on microglial activation phenotypes and neuroinflammation following TBI. We demonstrated that PKM2 expression was significantly increased during the acute and subacute phases of TBI, along with microglial activation. We demonstrated a specific mechanism by which tetramerization of PKM2 transitions microglial activation to an anti-inflammatory phenotype, which is used to maintain normal mitochondrial morphology and quality (Fig. 8). The distinct mechanisms by which shikonin and TEPP-46 affect microglial activation phenotype were compared, and we found that enhancing the interaction between PKM2 and MFN2 plays a partial role in the regulation of microglial phenotypic transitions. This was further confirmed *in vivo*, in which TEPP-46 exhibited a better treatment effect on neuronal loss and cognitive impairment following TBI compared to the inhibition of total PKM2 in microglia by shikonin.

Neuroinflammatory processes evolve over many years after TBI, leading to significant neuropsychiatric problems and neurodegenerative pathologies(Gyoneva and Ransohoff, 2015; Ng and Lee, 2019). As the resident innate immune cells in the CNS, microglia respond within minutes toward the sites of damage, where they can persist for many years following TBI(Jassam et al., 2017). Single-cell RNA sequencing

determined the contribution of microglia to neuropathology at 1-day post-injury, subacute (7-day-post injury), and chronic (30-day-post injury) time points(Witcher et al., 2021). In response to acute brain injury, microglia dynamically and temporally change their phenotypes, depending on different pathophysiological conditions. It has been reported that microglia/macrophages express both M1- and M2-like phenotypic markers early after TBI, but transient upregulation of the M2-like phenotype is replaced by a predominant M1- or mixed transitional phenotype at seven days post-injury(Kumar et al., 2016). The shift towards the M1-like and mixed transitional phenotypes was associated with increased neurodegeneration and promotion of the M2-like response, and attenuating the M1-like response may increase the likelihood of injury resolution(Hu et al., 2012). These results were consistent with those of the present study. We found that pro-inflammatory cytokines significantly increased at one-day post-injury and maintained a high level until seven days post-injury, along with significant microglial activation.

Many studies have aimed to elucidate the mechanisms of microglia/macrophage polarization, focusing primarily on the classic activation pathways such as JAK/STAT6/SOC3, NRF2/HO-1, and PPARγ,as well as the M2-microglia phenotype(Lan et al., 2017). Recently, multiple studies have revealed the importance of metabolic pathways in microglia(Scott et al., 2021). Microglia induce changes in their metabolic profiles in response to injury. In the M2-like phenotype, microglia rely more on OXPHOS for ATP production than in the M1-like phenotype. When activated into an M1-like phenotype, microglia rely more on anaerobic metabolism, a phenomenon known as the Warburg effect(Pan et al., 2019; Hu et al., 2020). PKM2 acts as a key metabolic enzyme, transcriptional regulator, and protein kinase and has been reported to mediate energy metabolism and mitochondrial morphology(Qi et al., 2017; Zhang et al., 2019). PKM2 has been observed to be unregulated in immunocytes of many inflammation-related diseases, such as ischemic stroke, colitis, and sepsis(Xie et al., 2016; Wang et al., 2017; Gao et al., 2020). Similarly, we observed that the expression of PKM2 was dramatically increased in microglia at three- and seven-days post-injury.

The monomeric or dimeric forms of PKM2 localize to the nucleus, which promotes glycolytic and inflammatory phenotypes. The tetrameric form of PKM2 is restricted to the cytosol and promotes glycolytic flux(Zhang et al., 2019). It has been reported that PKM2 translocates into the nucleus of $CD4^+$ T cells upon T cell receptor stimulation. PKM2 tetramerization by TEPP-46 blocks its nuclear translocation and engagement in glycolysis, thus inhibiting T cell activation, Th17 and Th1 polarization, and the development of experimental autoimmune encephalomyelitis in vivo(Angiari et al., 2020). Consistent with the well-characterized effect of TEPP-46 in promoting PKM2 tetramer formation and inhibiting its nuclear translocation(Anastasiou et al., 2012), we observed that TEPP-46 blocked PKM2 nuclear translocation and increased intracytoplasmic PKM2 levels in pro-inflammatory activated microglia. Studies have also shown that tetramerization of PKM2 and blocking its nuclear translocation by DASA-58 and TEPP-46 attenuates glycolysis and the pro-inflammatory M1-macrophage phenotype(Palsson-McDermott et al., 2015; Rao et al., 2022). These results are in accordance with our findings that tetramerization of PKM2 transitions microglial activation into an anti-inflammatory phenotype. Shikonin, a potent PKM2 inhibitor,

inhibits multiple functions of dimeric PKM2 in cancer cells and macrophages(Xie et al., 2016). Consistently, shikonin treatment inhibits microglial activation and attenuates neuroinflammation following TBI. Our results further support the hypothesis that the nuclear translocation of PKM2 is required for the generation of the pro-inflammatory M1 phenotype. Studies have suggested that inhibition of microglial PKM2 may significantly attenuate microglial activation and improve cognitive impairment in Alzheimer's disease(Pan et al., 2022) and lupus encephalopathy in mice(Lu et al., 2021). Our results are in agreement with these studies, which demonstrated that either inhibition of total PKM2 in microglia by shikonin or induction of tetramerization of PKM2 by TEEP-46 could ameliorate neuronal loss and cognitive impairment following TBI. Normal mitochondrial function is essential for maintaining metabolic pathways. Studies have shown that primary microglia exposed to LPS have increased mitochondrial fission, leading to more fragmentation than tubular mitochondria and metabolic reprogramming from oxidative phosphorylation to glycolysis(Nair et al., 2019). We also observed increased mitochondria exhibiting punctuated morphology and loss of mitochondrial membrane potential in pro-inflammatory activated microglia. The balance between mitochondrial fusion and fission maintains a normal mitochondrial morphology and function. The interaction between PKM2 and MFN2, a key regulator of mitochondrial fusion, has been well-studied in cancer cells(Li et al., 2019). It has been suggested that tetramerization of PKM2 can significantly enhance mitochondrial fusion and maintain tubular mitochondria(Scott et al., 2021). Furthermore, mTOR has been shown to increase the interaction between PKM2 and MFN2 by phosphorylating MFN2, thereby promoting mitochondrial fusion and OXPHOS and attenuating glycolysis(Li et al., 2019). In agreement with these results, we also demonstrated that tetramerization of PKM2 in pro-inflammatory activated microglia by TEPP-46 significantly enhanced the interaction of PKM2 with MFN2 and maintained the mitochondrial morphology and membrane potential. However, there are limitations in the present study as it is still unclear which specific mitochondrial function is affected by TEPP46.

An increasing number of studies have suggested that PKM2 is a potential target for therapeutic intervention in various acute and chronic inflammatory diseases(Lv et al., 2021; Zuo et al., 2021). According to existing reports, TEPP-46 and DASA-58 are the most widely used PKM2 activators, while shikonin and compound 3k are the most widely used PKM2 inhibitors(Palsson-McDermott et al., 2015; Kumar et al., 2020; Xu et al., 2020). As metabolic pathways change under different conditions in various cell types, PKM2 undergoes different post-translational modifications, which alter its cellular functions(Lee et al., 2022). Several studies have reported the effects of PKM2 activators and inhibitors on mitochondrial morphology and function. Kurt et al. demonstrated that in pulmonary hypertension fibroblasts, pharmacological inhibition of PKM2 glycolytic function with both TEPP-46 and shikonin reversed the glycolytic phenotype and rescued mitochondrial function(Zhang et al., 2017). However, PKM2 knockdown dramatically increased mitochondrial fragmentation in cancer cells, as determined by confocal and electron microscopy(Li et al., 2019). It has also been reported that shikonin induces necroptosis in glioma cells by increasing mitochondrial ROS levels(Lu et al., 2017). In this study, we demonstrated that shikonin and siPKM2 significantly suppressed pro-inflammatory microglial activation, without improving mitochondrial morphology. Moreover, TEPP46 exhibited a better treatment effect,

indicating that the protection of mitochondrial qualification following TBI by enhancing the interaction of PKM2 with MFN2 contributed to increased treatment efficiency.

Conclusion

Collectively, our results suggest that the nuclear translocation of PKM2 is required for the generation of a pro-inflammatory phenotype in microglia. Tetramerization of PKM2 promotes microglial transformation into an anti-inflammatory phenotype by providing mitochondrial protection through interactions between PKM2 and MFN2. This study confirmed that PKM2 is an important regulator of microglial activation and neuroinflammation, and should be considered as a target for further research on therapeutic interventions in TBI.

Abbreviations

TBI
Traumatic Brain Injury
PKM2
Pyruvate kinase isoform M2
SK
Shikonin
FCT
Fear conditioning test
IL-1β
Interleukin-1β
IL-6
Interleukin-6
TNF-α
tumor necrosis factor-α
iNOS
Inducible nitric oxide synthase
CNS
Central nervous system
BSA
Bovine serum albumin
DAPI
2-(4-Amidinophenyl)-1H-indole-6-carboxamidine
Iba1
Ionized calcium-binding adaptor molecule-1
NEUN
neuronal nuclei

JC-1
5,5',6,6'-Tetrachloro-1,1',3,3'-tetraethyl-imidacarbocyanine
LPS
Lipopolysaccharide
DSS
Disuccinimidyl suberate
MFN2
Mitofusin2
SDS-PAGE
Sodium dodecyl sulfate-polyacrylamide gel electrophoresis
ELISA
Enzyme-linked immunosorbent assay
BrdU
5-bromo-2’-deoxyuridine
TEM
Transmission electron microscopy

Declarations

Funding

This work was supported by the National Natural Science Foundation of China (grant nos. 81571240 and 81771171), Science and Technology Development Fund of Nanjing Medical University (NMUB20210045), and Nanjing Health Science and Technology Development Project (ZKX21038).

Conflicts of interest

The authors declare no competing interests.

Availability of data and material

Data included in this study are available upon request by contact with the corresponding author.

Code availability

Not applicable

Authors' contributions

YF and Y-ZR designed the experiments, obtained resources, and acquired funding. Y-ZR, H-YZ, X-JZ, L-Y Z, XL and Z-YZ participated in protocol execution, data generation, collection, and analysis. Y-ZR, H-YZ and H-WZ drafted the manuscript. All authors read and approved the final version of the manuscript.

Ethics approval

All animal protocols were approved by the Ethics Committee of Nanjing Medical University College and the National Institutes of Health Guide for the Care and Use of Laboratory Animals (#IACUC-2011010).

Consent to participate

Not applicable

Consent for publication

Not applicable

Conflict of interest disclosure: This research was conducted in the absence of any commercial or financial relationships that could be construed as potential conflicts of interest.

References

1. Ahluwalia M, Kumar M, Ahluwalia P, Rahimi S, Vender JR, Raju RP, Hess DC, Baban B, Vale FL, Dhandapani KM, Vaibhav K (2021) Rescuing mitochondria in traumatic brain injury and intracerebral hemorrhages - A potential therapeutic approach. Neurochem Int 150:105192. https://doi.org/10.1016/j.neuint.2021.105192
2. Alquraishi M, Puckett DL, Alani DS, Humidat AS, Frankel VD, Donohoe DR, Whelan J, Bettaieb A (2019) Pyruvate kinase M2: A simple molecule with complex functions. Free Radic Biol Med 143:176–192. https://doi.org/10.1016/j.freeradbiomed.2019.08.007
3. Anastasiou D et al (2012) Pyruvate kinase M2 activators promote tetramer formation and suppress tumorigenesis. Nat Chem Biol 8:839–847. https://doi.org/10.1038/nchembio.1060
4. Angiari S, Runtsch MC, Sutton CE, Palsson-McDermott EM, Kelly B, Rana N, Kane H, Papadopoulou G, Pearce EL, Mills KHG, O'Neill LAJ (2020) Pharmacological Activation of Pyruvate Kinase M2 Inhibits CD4(+) T Cell Pathogenicity and Suppresses Autoimmunity. Cell Metab 31:391–405. e398.https://doi.org/10.1016/j.cmet.2019.10.015
5. Anthonymuthu TS, Kenny EM, Bayir H (2016) Therapies targeting lipid peroxidation in traumatic brain injury. Brain Res 1640:57–76. https://doi.org/10.1016/j.brainres.2016.02.006
6. Bernier LP, York EM, MacVicar BA (2020) Immunometabolism in the Brain: How Metabolism Shapes Microglial Function. Trends Neurosci 43:854–869. https://doi.org/10.1016/j.tins.2020.08.008
7. Best L, Ghadery C, Pavese N, Tai YF, Strafella AP (2019) New and Old TSPO PET Radioligands for Imaging Brain Microglial Activation in Neurodegenerative Disease. Curr Neurol Neurosci Rep 19:24. https://doi.org/10.1007/s11910-019-0934-y
8. Blum JE, Gheller BJ, Benvie A, Field MS, Panizza E, Vacanti NM, Berry D, Thalacker-Mercer A (2021) Pyruvate Kinase M2 Supports Muscle Progenitor Cell Proliferation but Is Dispensable for Skeletal Muscle Regeneration after Injury. J Nutr 151:3313–3328. https://doi.org/10.1093/jn/nxab251

9. Carneiro CFD, Moulin TC, Macleod MR, Amaral OB (2018) Effect size and statistical power in the rodent fear conditioning literature - A systematic review. PLoS ONE 13:e0196258. https://doi.org/10.1371/journal.pone.0196258
10. Chao H, Lin C, Zuo Q, Liu Y, Xiao M, Xu X, Li Z, Bao Z, Chen H, You Y, Kochanek PM, Yin H, Liu N, Kagan VE, Bayir H, Ji J (2019) Cardiolipin-Dependent Mitophagy Guides Outcome after Traumatic Brain Injury. J Neurosci 39:1930–1943. https://doi.org/10.1523/JNEUROSCI.3415-17.2018
11. Cibelli M, Fidalgo AR, Terrando N, Ma D, Monaco C, Feldmann M, Takata M, Lever IJ, Nanchahal J, Fanselow MS, Maze M (2010) Role of interleukin-1beta in postoperative cognitive dysfunction. Ann Neurol 68:360–368. https://doi.org/10.1002/ana.22082
12. Collaborators GBDN (2019) Global, regional, and national burden of neurological disorders, 1990–2016: a systematic analysis for the Global Burden of Disease Study 2016. Lancet Neurol 18:459–480. https://doi.org/10.1016/S1474-4422(18)30499-X
13. Dorsett CR, McGuire JL, DePasquale EA, Gardner AE, Floyd CL, McCullumsmith RE (2017) Glutamate Neurotransmission in Rodent Models of Traumatic Brain Injury. J Neurotrauma 34:263–272. https://doi.org/10.1089/neu.2015.4373
14. Fairley LH, Wong JH, Barron AM (2021) Mitochondrial Regulation of Microglial Immunometabolism in Alzheimer's Disease. Front Immunol 12:624538. https://doi.org/10.3389/fimmu.2021.624538
15. Gao CL, Hou GG, Liu J, Ru T, Xu YZ, Zhao SY, Ye H, Zhang LY, Chen KX, Guo YW, Pang T, Li XW (2020) Synthesis and Target Identification of Benzoxepane Derivatives as Potential Anti-Neuroinflammatory Agents for Ischemic Stroke. Angew Chem Int Ed Engl 59:2429–2439. https://doi.org/10.1002/anie.201912489
16. Gong Z, Pan J, Shen Q, Li M, Peng Y (2018) Mitochondrial dysfunction induces NLRP3 inflammasome activation during cerebral ischemia/reperfusion injury. J Neuroinflammation 15:242. https://doi.org/10.1186/s12974-018-1282-6
17. Gyoneva S, Ransohoff RM (2015) Inflammatory reaction after traumatic brain injury: therapeutic potential of targeting cell-cell communication by chemokines. Trends Pharmacol Sci 36:471–480. https://doi.org/10.1016/j.tips.2015.04.003
18. Hu X, Li P, Guo Y, Wang H, Leak RK, Chen S, Gao Y, Chen J (2012) Microglia/macrophage polarization dynamics reveal novel mechanism of injury expansion after focal cerebral ischemia. Stroke 43:3063–3070. https://doi.org/10.1161/STROKEAHA.112.659656
19. Hu Y, Mai W, Chen L, Cao K, Zhang B, Zhang Z, Liu Y, Lou H, Duan S, Gao Z (2020) mTOR-mediated metabolic reprogramming shapes distinct microglia functions in response to lipopolysaccharide and ATP. Glia 68:1031–1045. https://doi.org/10.1002/glia.23760
20. Jassam YN, Izzy S, Whalen M, McGavern DB, El Khoury J (2017) Neuroimmunology of Traumatic Brain Injury: Time for a Paradigm Shift. Neuron 95:1246–1265. https://doi.org/10.1016/j.neuron.2017.07.010
21. Kong Q, Li N, Cheng H, Zhang X, Cao X, Qi T, Dai L, Zhang Z, Chen X, Li C, Li Y, Xue B, Fang L, Liu L, Ding Z (2019) HSPA12A Is a Novel Player in Nonalcoholic Steatohepatitis via Promoting Nuclear

PKM2-Mediated M1 Macrophage Polarization. Diabetes 68:361–376. https://doi.org/10.2337/db18-0035

22. Kumar A, Alvarez-Croda DM, Stoica BA, Faden AI, Loane DJ (2016) Microglial/Macrophage Polarization Dynamics following Traumatic Brain Injury. J Neurotrauma 33:1732–1750. https://doi.org/10.1089/neu.2015.4268
23. Kumar A, Gupta P, Rana M, Chandra T, Dikshit M, Barthwal MK (2020) Role of pyruvate kinase M2 in oxidized LDL-induced macrophage foam cell formation and inflammation. J Lipid Res 61:351–364. https://doi.org/10.1194/jlr.RA119000382
24. Lan X, Han X, Li Q, Yang QW, Wang J (2017) Modulators of microglial activation and polarization after intracerebral haemorrhage. Nat Rev Neurol 13:420–433. https://doi.org/10.1038/nrneurol.2017.69
25. Lee YB, Min JK, Kim JG, Cap KC, Islam R, Hossain AJ, Dogsom O, Hamza A, Mahmud S, Choi DR, Kim YS, Koh YH, Kim HA, Chung WS, Suh SW, Park JB (2022) Multiple functions of pyruvate kinase M2 in various cell types. J Cell Physiol 237:128–148. https://doi.org/10.1002/jcp.30536
26. Li T, Han J, Jia L, Hu X, Chen L, Wang Y (2019) PKM2 coordinates glycolysis with mitochondrial fusion and oxidative phosphorylation. Protein Cell 10:583–594. https://doi.org/10.1007/s13238-019-0618-z
27. Li X, Tian BM, Deng DK, Liu F, Zhou H, Kong DQ, Qu HL, Sun LJ, He XT, Chen FM (2022) LncRNA GACAT2 binds with protein PKM1/2 to regulate cell mitochondrial function and cementogenesis in an inflammatory environment. Bone Res 10:29. https://doi.org/10.1038/s41413-022-00197-x
28. Lu B, Gong X, Wang ZQ, Ding Y, Wang C, Luo TF, Piao MH, Meng FK, Chi GF, Luo YN, Ge PF (2017) Shikonin induces glioma cell necroptosis in vitro by ROS overproduction and promoting RIP1/RIP3 necrosome formation. Acta Pharmacol Sin 38:1543–1553. https://doi.org/10.1038/aps.2017.112
29. Lu L, Wang H, Liu X, Tan L, Qiao X, Ni J, Sun Y, Liang J, Hou Y, Dou H (2021) Pyruvate kinase isoform M2 impairs cognition in systemic lupus erythematosus by promoting microglial synaptic pruning via the beta-catenin signaling pathway. J Neuroinflammation 18:229. https://doi.org/10.1186/s12974-021-02279-9
30. Lv X, Zhou H, Hu K, Lin L, Yang Y, Li L, Tang L, Huang J, Shen Y, Jiang R, Wan J, Zhang L (2021) Activation of PKM2 metabolically controls fulminant liver injury via restoration of pyruvate and reactivation of CDK1. Pharmacol Res 172:105838. https://doi.org/10.1016/j.phrs.2021.105838
31. Maas AI, Stocchetti N, Bullock R (2008) Moderate and severe traumatic brain injury in adults. Lancet Neurol 7:728–741. https://doi.org/10.1016/S1474-4422(08)70164-9
32. Maas AIR et al (2017) Traumatic brain injury: integrated approaches to improve prevention, clinical care, and research. Lancet Neurol 16:987–1048. https://doi.org/10.1016/S1474-4422(17)30371-X
33. Mishra P, Chan DC (2014) Mitochondrial dynamics and inheritance during cell division, development and disease. Nat Rev Mol Cell Biol 15:634–646. https://doi.org/10.1038/nrm3877
34. Nagy AM, Fekete R, Horvath G, Koncsos G, Kriston C, Sebestyen A, Giricz Z, Kornyei Z, Madarasz E, Tretter L (2018) Versatility of microglial bioenergetic machinery under starving conditions. Biochim

Biophys Acta Bioenerg 1859:201–214. https://doi.org/10.1016/j.bbabio.2017.12.002

35. Nair S, Sobotka KS, Joshi P, Gressens P, Fleiss B, Thornton C, Mallard C, Hagberg H (2019) Lipopolysaccharide-induced alteration of mitochondrial morphology induces a metabolic shift in microglia modulating the inflammatory response in vitro and in vivo. Glia 67:1047–1061. https://doi.org/10.1002/glia.23587
36. Ng SY, Lee AYW (2019) Traumatic Brain Injuries: Pathophysiology and Potential Therapeutic Targets. Front Cell Neurosci 13:528. https://doi.org/10.3389/fncel.2019.00528
37. Okello A, Edison P, Archer HA, Turkheimer FE, Kennedy J, Bullock R, Walker Z, Kennedy A, Fox N, Rossor M, Brooks DJ (2009) Microglial activation and amyloid deposition in mild cognitive impairment: a PET study. Neurology 72:56–62. https://doi.org/10.1212/01.wnl.0000338622.27876.0d
38. Palsson-McDermott EM, Curtis AM, Goel G, Lauterbach MA, Sheedy FJ, Gleeson LE, van den Bosch MW, Quinn SR, Domingo-Fernandez R, Johnston DG, Jiang JK, Israelsen WJ, Keane J, Thomas C, Clish C, Vander Heiden M, Xavier RJ, O'Neill LA (2015) Pyruvate kinase M2 regulates Hif-1alpha activity and IL-1beta induction and is a critical determinant of the warburg effect in LPS-activated macrophages. Cell Metab 21:65–80. https://doi.org/10.1016/j.cmet.2014.12.005
39. Pan RY, Ma J, Kong XX, Wang XF, Li SS, Qi XL, Yan YH, Cheng J, Liu Q, Jin W, Tan CH, Yuan Z (2019) Sodium rutin ameliorates Alzheimer's disease-like pathology by enhancing microglial amyloid-beta clearance. Sci Adv 5:eaau6328. https://doi.org/10.1126/sciadv.aau6328
40. Pan RY, He L, Zhang J, Liu X, Liao Y, Gao J, Liao Y, Yan Y, Li Q, Zhou X, Cheng J, Xing Q, Guan F, Zhang J, Sun L, Yuan Z (2022) Positive feedback regulation of microglial glucose metabolism by histone H4 lysine 12 lactylation in Alzheimer's disease. Cell Metab 34:634–648. e636.https://doi.org/10.1016/j.cmet.2022.02.013
41. Peruzzotti-Jametti L, Willis CM, Hamel R, Krzak G, Pluchino S (2021) Metabolic Control of Smoldering Neuroinflammation. Front Immunol 12:705920. https://doi.org/10.3389/fimmu.2021.705920
42. Pickles S, Vigie P, Youle RJ (2018) Mitophagy and Quality Control Mechanisms in Mitochondrial Maintenance. Curr Biol 28:R170. R185.https://doi.org/10.1016/j.cub.2018.01.004
43. Qi W et al (2017) Pyruvate kinase M2 activation may protect against the progression of diabetic glomerular pathology and mitochondrial dysfunction. Nat Med 23:753–762. https://doi.org/10.1038/nm.4328
44. Rao J, Wang H, Ni M, Wang Z, Wang Z, Wei S, Liu M, Wang P, Qiu J, Zhang L, Wu C, Shen H, Wang X, Cheng F, Lu L (2022) FSTL1 promotes liver fibrosis by reprogramming macrophage function through modulating the intracellular function of PKM2. Gut 71:2539–2550. https://doi.org/10.1136/gutjnl-2021-325150
45. Ren YZ, Zhang BZ, Zhao XJ, Zhang ZY (2020) Resolvin D1 ameliorates cognitive impairment following traumatic brain injury via protecting astrocytic mitochondria. J Neurochem 154:530–546. https://doi.org/10.1111/jnc.14962

46. Sarkar S, Malovic E, Harishchandra DS, Ghaisas S, Panicker N, Charli A, Palanisamy BN, Rokad D, Jin H, Anantharam V, Kanthasamy A, Kanthasamy AG (2017) Mitochondrial impairment in microglia amplifies NLRP3 inflammasome proinflammatory signaling in cell culture and animal models of Parkinson's disease. NPJ Parkinsons Dis 3:30. https://doi.org/10.1038/s41531-017-0032-2
47. Scott MC, Bedi SS, Olson SD, Sears CM, Cox CS (2021) Microglia as therapeutic targets after neurological injury: strategy for cell therapy. Expert Opin Ther Targets 25:365–380. https://doi.org/10.1080/14728222.2021.1934447
48. Terrando N, Yang T, Ryu JK, Newton PT, Monaco C, Feldmann M, Ma D, Akassoglou K, Maze M (2015) Stimulation of the alpha7 nicotinic acetylcholine receptor protects against neuroinflammation after tibia fracture and endotoxemia in mice. Mol Med 20:667–675. https://doi.org/10.2119/molmed.2014.00143
49. Wang F, Wang K, Xu W, Zhao S, Ye D, Wang Y, Xu Y, Zhou L, Chu Y, Zhang C, Qin X, Yang P, Yu H (2017) SIRT5 Desuccinylates and Activates Pyruvate Kinase M2 to Block Macrophage IL-1beta Production and to Prevent DSS-Induced Colitis in Mice. Cell Rep 19:2331–2344. https://doi.org/10.1016/j.celrep.2017.05.065
50. Witcher KG, Bray CE, Chunchai T, Zhao F, O'Neil SM, Gordillo AJ, Campbell WA, McKim DB, Liu X, Dziabis JE, Quan N, Eiferman DS, Fischer AJ, Kokiko-Cochran ON, Askwith C, Godbout JP (2021) Traumatic Brain Injury Causes Chronic Cortical Inflammation and Neuronal Dysfunction Mediated by Microglia. J Neurosci 41:1597–1616. https://doi.org/10.1523/JNEUROSCI.2469-20.2020
51. Xie M, Yu Y, Kang R, Zhu S, Yang L, Zeng L, Sun X, Yang M, Billiar TR, Wang H, Cao L, Jiang J, Tang D (2016) PKM2-dependent glycolysis promotes NLRP3 and AIM2 inflammasome activation. Nat Commun 7:13280. https://doi.org/10.1038/ncomms13280
52. Xu F, Guo M, Huang W, Feng L, Zhu J, Luo K, Gao J, Zheng B, Kong LD, Pang T, Wu X, Xu Q (2020) Annexin A5 regulates hepatic macrophage polarization via directly targeting PKM2 and ameliorates NASH. Redox Biol 36:101634. https://doi.org/10.1016/j.redox.2020.101634
53. Yang W, Zheng Y, Xia Y, Ji H, Chen X, Guo F, Lyssiotis CA, Aldape K, Cantley LC, Lu Z (2012) ERK1/2-dependent phosphorylation and nuclear translocation of PKM2 promotes the Warburg effect. Nat Cell Biol 14:1295–1304. https://doi.org/10.1038/ncb2629
54. Yi Z, Wu Y, Zhang W, Wang T, Gong J, Cheng Y, Miao C (2020) Activator-Mediated Pyruvate Kinase M2 Activation Contributes to Endotoxin Tolerance by Promoting Mitochondrial Biogenesis. Front Immunol 11:595316. https://doi.org/10.3389/fimmu.2020.595316
55. Zhang H, Wang D, Li M, Plecita-Hlavata L, D'Alessandro A, Tauber J, Riddle S, Kumar S, Flockton A, McKeon BA, Frid MG, Reisz JA, Caruso P, El Kasmi KC, Jezek P, Morrell NW, Hu CJ, Stenmark KR (2017) Metabolic and Proliferative State of Vascular Adventitial Fibroblasts in Pulmonary Hypertension Is Regulated Through a MicroRNA-124/PTBP1 (Polypyrimidine Tract Binding Protein 1)/Pyruvate Kinase Muscle Axis. Circulation 136:2468–2485. https://doi.org/10.1161/CIRCULATIONAHA.117.028069

56. Zhang Y, Chen K, Sloan SA, Bennett ML, Scholze AR, O'Keeffe S, Phatnani HP, Guarnieri P, Caneda C, Ruderisch N, Deng S, Liddelow SA, Zhang C, Daneman R, Maniatis T, Barres BA, Wu JQ (2014) An RNA-sequencing transcriptome and splicing database of glia, neurons, and vascular cells of the cerebral cortex. J Neurosci 34:11929–11947. https://doi.org/10.1523/JNEUROSCI.1860-14.2014
57. Zhang Z, Deng X, Liu Y, Liu Y, Sun L, Chen F (2019) PKM2, function and expression and regulation. Cell Biosci 9:52. https://doi.org/10.1186/s13578-019-0317-8
58. Zuo J, Tang J, Lu M, Zhou Z, Li Y, Tian H, Liu E, Gao B, Liu T, Shao P (2021) Glycolysis Rate-Limiting Enzymes: Novel Potential Regulators of Rheumatoid Arthritis Pathogenesis. Front Immunol 12:779787. https://doi.org/10.3389/fimmu.2021.779787

Tables

Table 1 Quantitative RT-PCR primers

Gene	Reverse primers	Forward primers
Actin	TGGAATCCTGTGTGGCATCCATGAAA	TAAAACGCAGCTCAGTAACAGTCCG
TNF-α	CAGGCGGTGCCTATGTCTC	CGATCACCCCGAAGTTCAGTAG
IL-6	CTGCAAGAGACTTCCATCCAG	AGTGGTATAGACAGGTCTGTTGG
IL-4	ATCATCGGCATTTTGAACGAGG	TGCAGCTCCATGAGAACACTA
IL-10	CTTACTGACTGGCATGAGGATCA	GCAGCTCTAGGAGCATGTGG
TGF-β	CCACCTGCAAGACCATCGAC	CTGGCGAGCCTTAGTTTGGAC
iNOS	TCTATACCACTTCACAAGTCGGA	GAATTGCCATTGCACAACTCTTT
PKM2	CGCCTGGACATTGACTCTG	GAAATTCAGCCGAGCCACATT
siPKM2(1)	GCCACAGAAAGCUUUGCAUTT	AUGCAAAGCUUUCUGUGGCTT
siPKM2(2)	GCAAGAACAUCAAGAUCAUTT	AUGAUCUUGAUGUUCUUGCTT
siPKM2(3)	GUGGAGGCCUCUUAUAAGUTT	ACUUAUAAGAGGCCUCCACTT
siMFN2(1)	GCGGGUUUAUUGCCUAGAATT	AUGCAAAGCUUUCUGUGGCTT
siMFN2(2)	CUGCCAUGAACAAGAAAGUTT	ACUUUCUUGUUCAUGGCAGTT
siMFN2(3)	CUGCGAAUUAAGCAGAUUATT	UAAUCUGCUUAAUUCGCAGTT

Figures

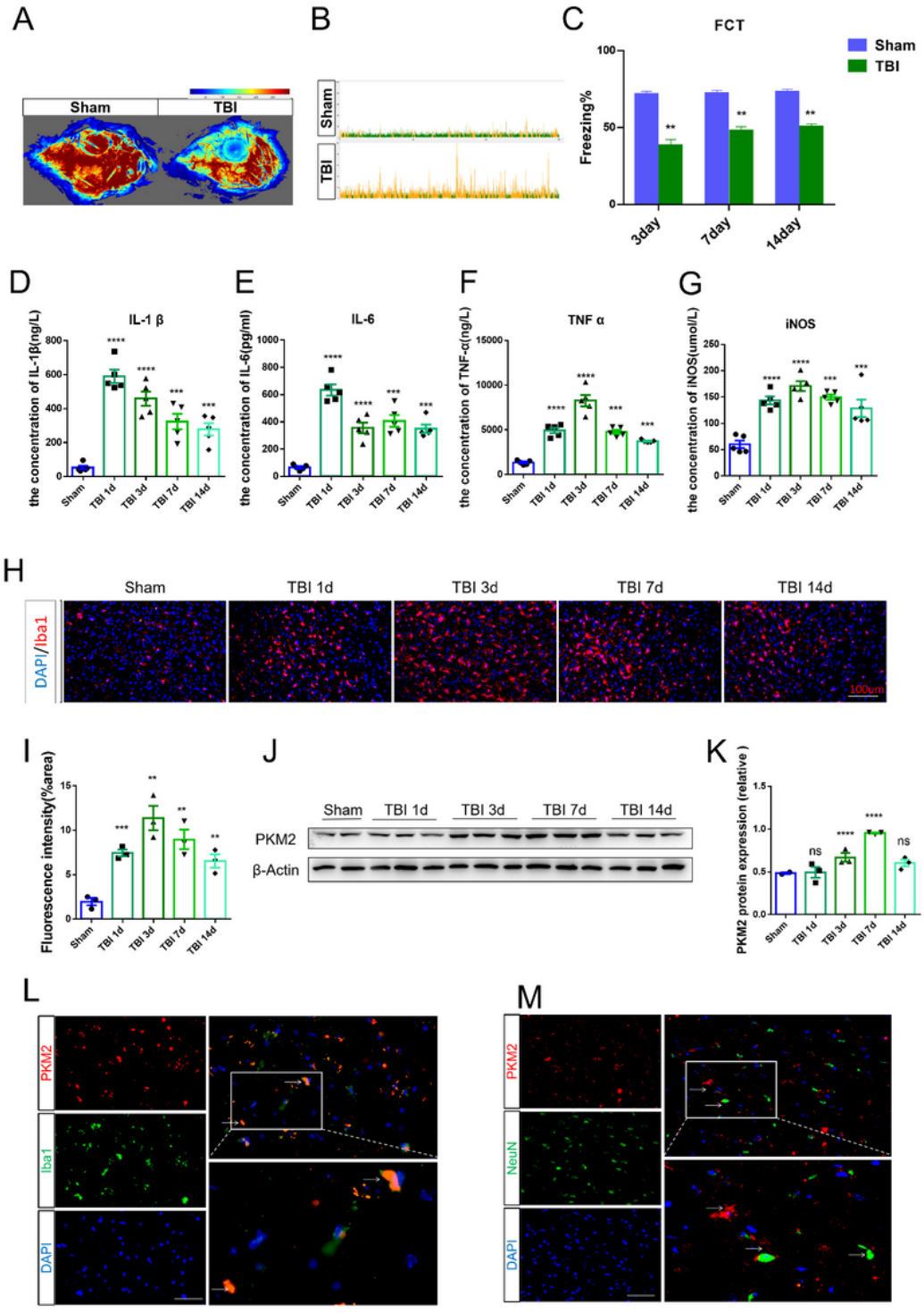

Figure 1

The expression of PKM2 increased and located in microglia in peri-contusional cortex following TBI. **A.**Representative cerebral blood flow photographs of whole brains in the sham and TBI group. **B-C.** Contextual fear conditioning at 3-, 7- and 14-days post-injury. **D-G.** Pro-inflammatory cytokines IL-1β (**D**), IL-6 (**E**), TNF-α(**F**), iNOS (**G**) in peri-contusional cortex at 1-, 3- ,7-, and 14-days post-injury. **H-I.** Immunofluorescence staning of Iba1(green) at 1-, 3-, 7- and 14-days post-injury. Representative images

showing Iba1 staining, (Scale bar=100 μm) (**H**). Statistical analysis of Iba1 expression(**I**). **J-K**. Western blot bands and densitometry of PKM2 in peri-contusional cortex following TBI. **L-M** The colocalization of **(L)** Iba1 (microglia marker, green) and **(M)** NeuN (neuronal marker, green) with PKM2 (red) in peri-contusional cortex at 7 post-injury (Scale bar=100 μm). Sample size: n=5/group for Elisa test, n=3/group for Western blotting, n=3/groupfor immunofluorescence staining. The data are expressed as the mean score ± SD; **P* < 0.05, ***P* < 0.01, ****P*< 0.001, *****P* < 0.001 vs sham group.

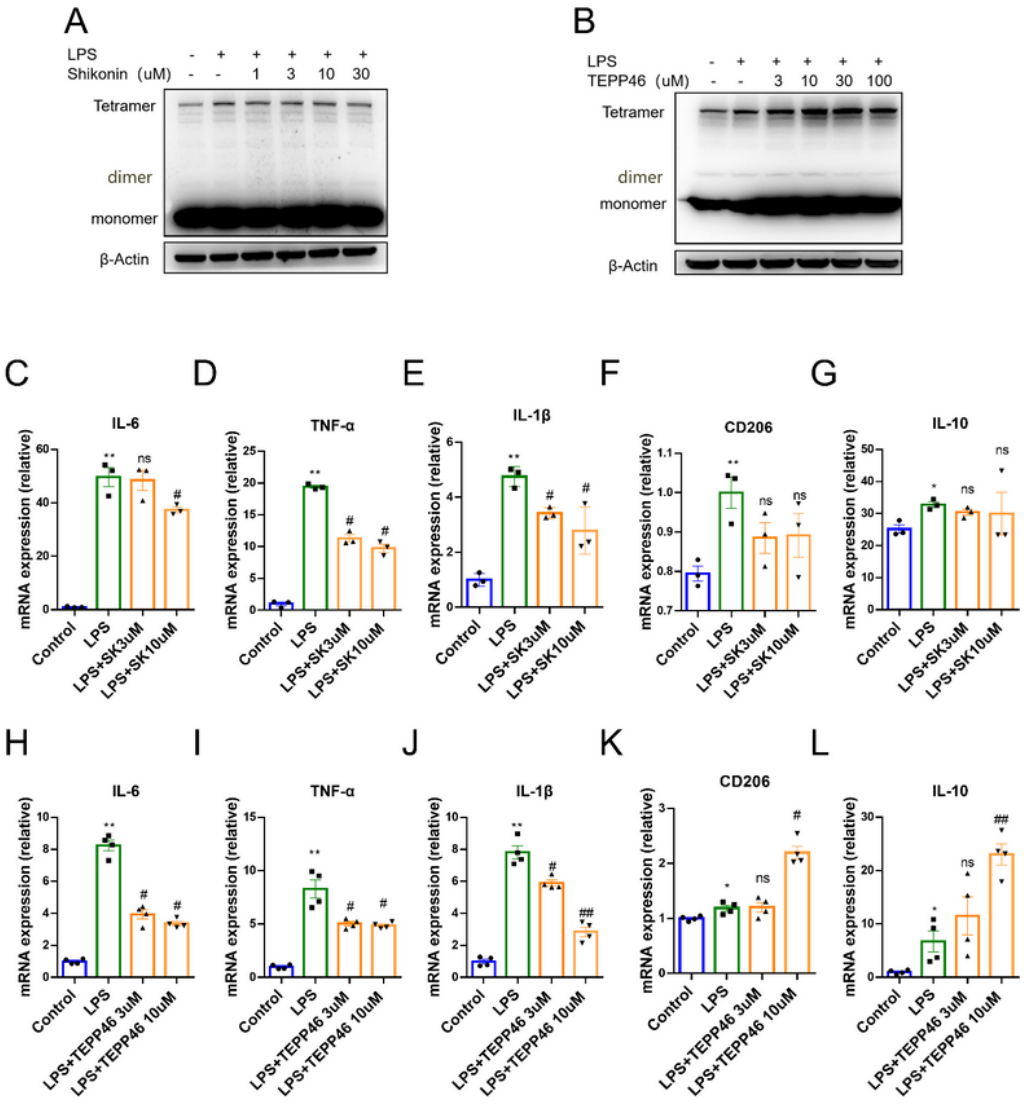

Figure 2

Tetramerization of PKM2 by TEPP-46 tend to transit microglia activation to anti-inflammation state. **A-B**. Cross linking (500 mM DSS) and western blot of endogenous PKM2 in Primary microglia. Primary microglia were pretreated with shikonin (**A**) and TEPP-46 (**B**) as indicated. **C-E.** Primary microglia was cultured and treated with LPS (1 μM, 12 h) and shikonin as indicated. qPCR analysis of the expression of pro-inflammatory cytokines IL-6 (**C**), TNF-α (**D**), IL-1β (**E**). **F-G.** anti-inflammatory cytokines CD206 (**F**), IL-10 (**G**). **H-J.** Primary microglia was cultured and treated with LPS (1 μM, 12 h) and TEPP46 as indicated. qPCR analysis showing that the expression of pro-inflammatory cytokines IL-6 (**H**), TNF-α (**I**), IL-1β (**J**). **K-L.** anti-inflammatory cytokines CD206 (**K**), IL-10 (**L**). Sample size: n=3-4/group for qPCR. The data are expressed as the means ± SD; $*P < 0.05$, $**P < 0.01$ vs control group. $^{\#}P < 0.05$, $^{\#\#}P < 0.01$ vs LPS group.

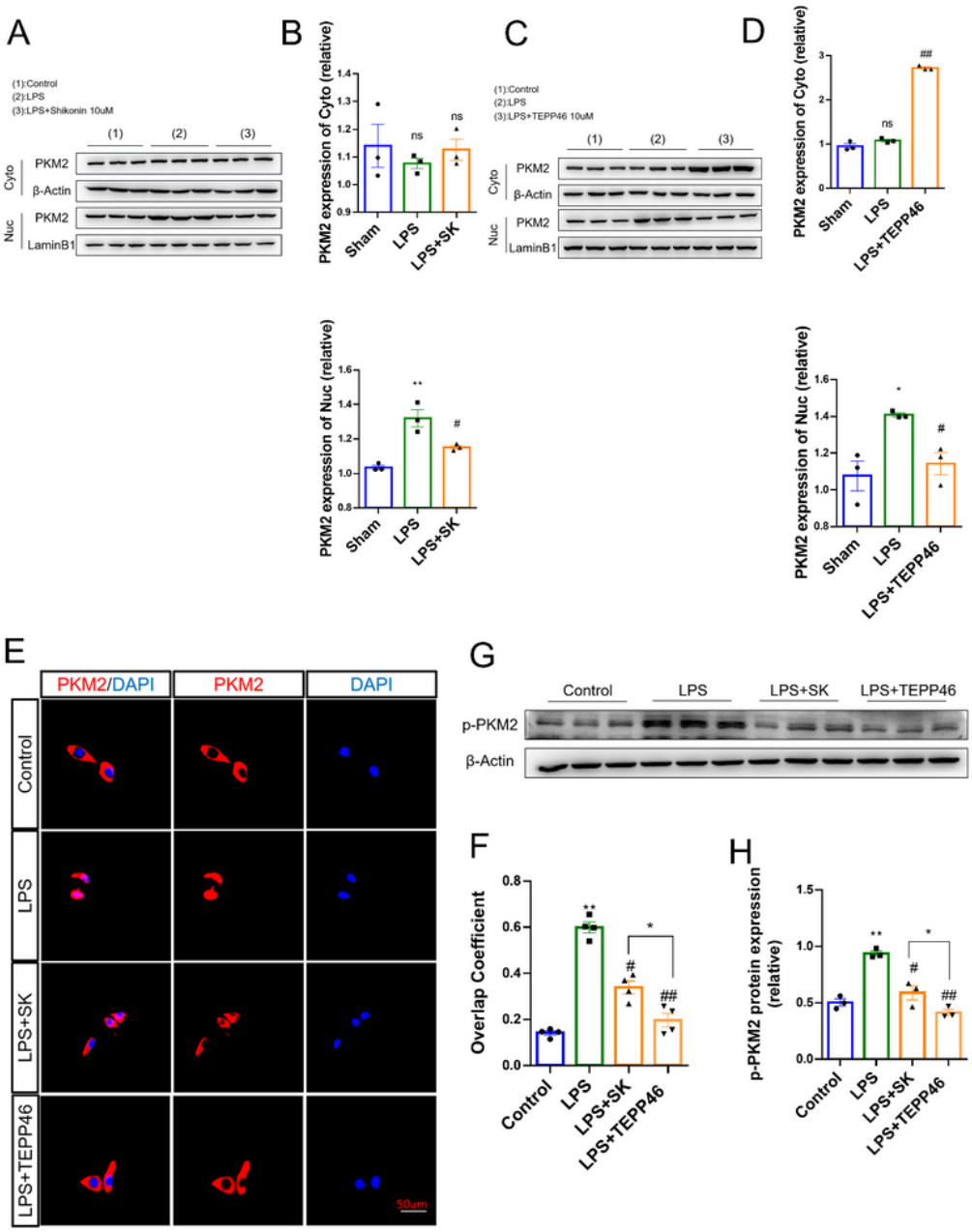

Figure 3

The effect of shikonin and TEPP-46 treatment on PKM2 subcellular localization in activated BV2 microglia. **A-D**. Cells were harvested shikonin 10 μM for 30 min (**A-B**) or TEPP-46 10 μM for 12 h (**C-D**) following LPS 1 μM for 12 h. Cytosol and nuclear fractionations were subjected to immunoblotting with PKM2 antibody. **E-F.** Immunofluorescence staining of PKM2 (red) in LPS-induced microglia with shikonin 10 μM or TEPP-46 10 μM treatment as above, Scale bar=50 μm. Representative images showing PKM2

staining (**E**). Statistical analysis of the intracellular and intranuclear ratio (**F**). **G-H.** Western blot analysis of p-PKM2 (Y-105) expression in primary microglia after shikonin and TEPP-46 treatment following LPS 1 μM for 12 h. Sample size:n=3/group for Western blotting, n=3/group for immunofluorescence staining.The data are presented as the means ± SD; **P* < 0.05, ***P* < 0.01vs control group. $^{\#}P < 0.05$, $^{\#\#}P < 0.01$ vs LPS group.

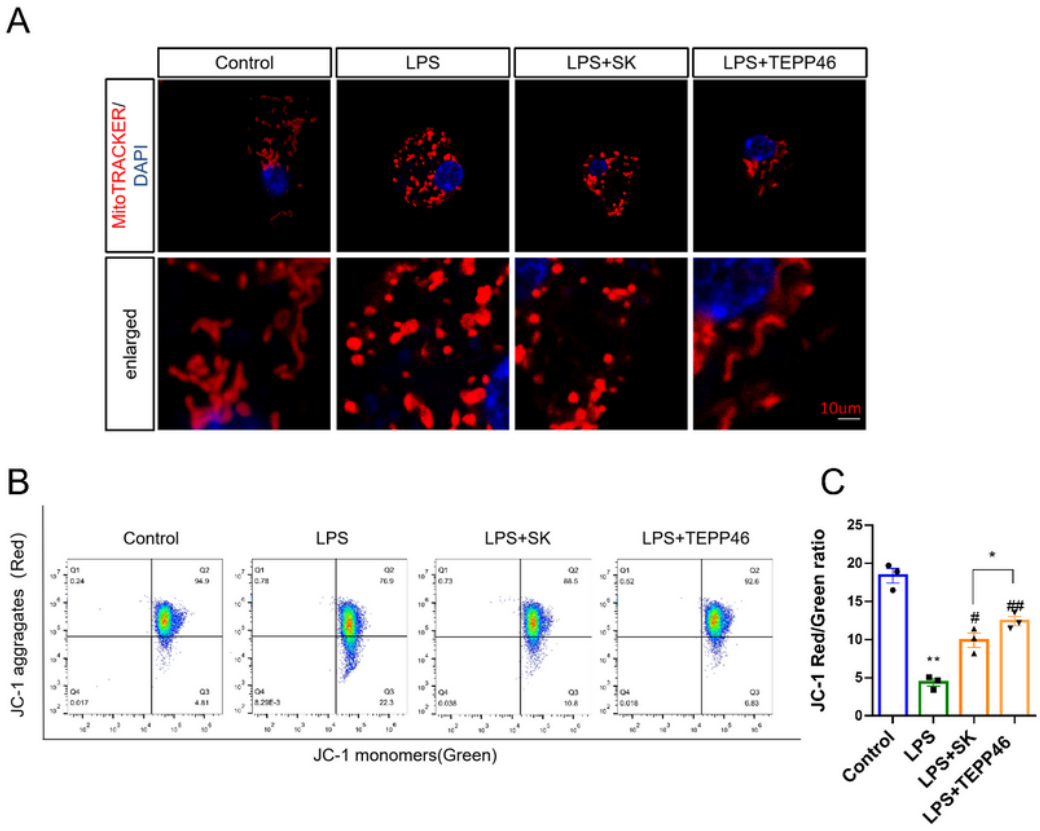

Figure 4

Down-regulation of PKM2 dimer and tetramer by shikonin increases mitochondrial fragmentation, but TEPP-46 induces PKM2 tetramerization can successfully maintain mitochondrial morphology. Primary microglia were cultured and treated with LPS (1 μM, 12 h) and with shikonin 10 μM or TEPP-46 10 μM. **A.** Representative changes in mitochondrial morphology were detected between groups. Images of mitochondria (red) and nuclei (blue) were obtained by confocal microscopy. Magnification, 63, zoom 2.0, Scale bar=10 μm. **B.** Analysis of the mitochondrial membrane potential (mtΔΨ) in primary microglia as indicated treatment. Representative images showing flow cytometry analysis of JC-1 staining. **C.** Statistical analysis of the JC-1 aggregate ratio (red/green). Sample size: n=3/group for MitoTracrker Red staining, n=3/group for flow cytometry analysis. The data are presented as the means ± SD; $*P < 0.05$, $**P < 0.01$vs control group. $^{\#}P < 0.05$, $^{\#\#}P < 0.01$ vs LPS group.

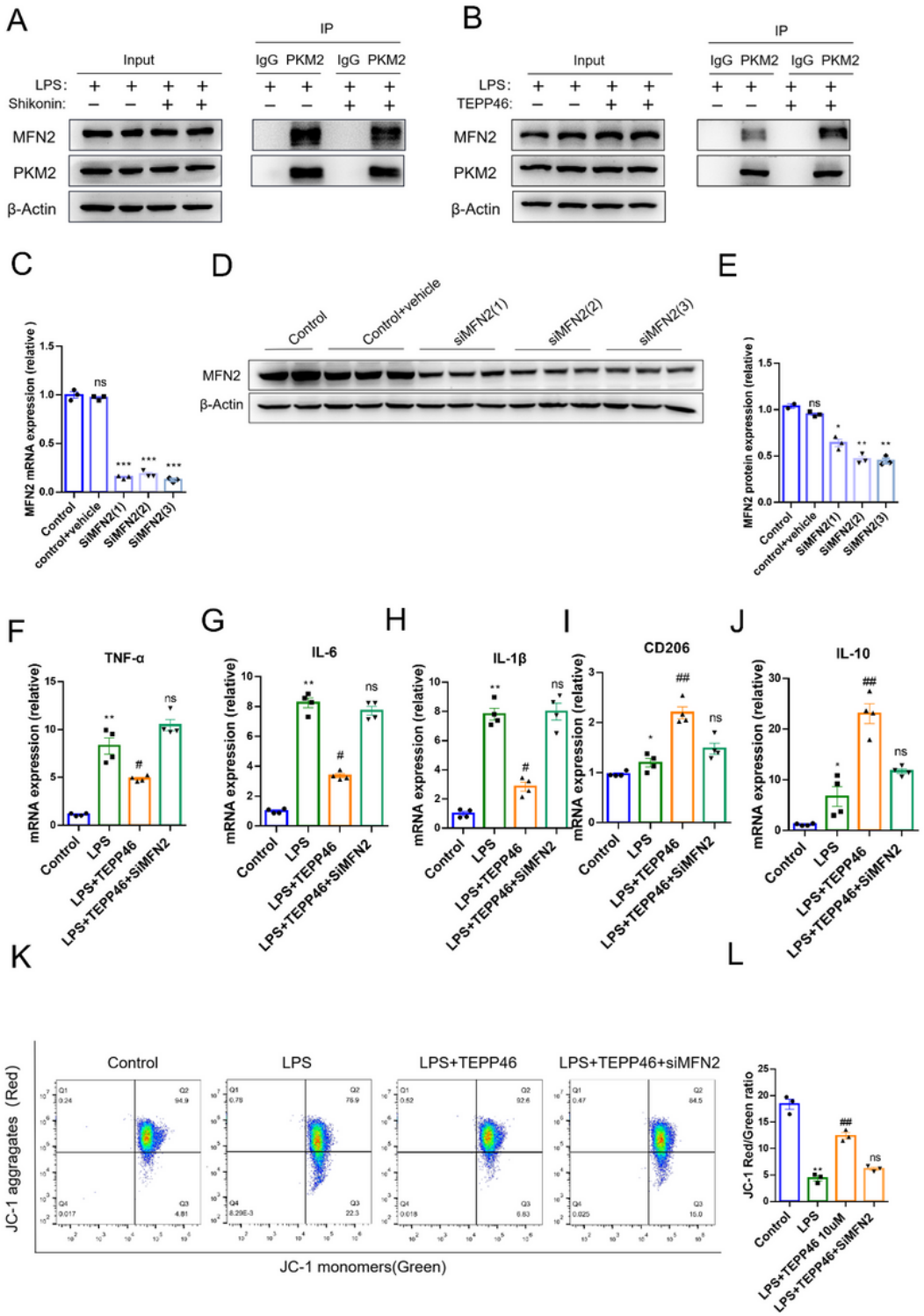

Figure 5

Promoting aggregation of dimer to tetramer in microglia enhance the interaction of PKM2 with MFN2. **A-B.** Co-IP showing the interaction of endogenous PKM2 and MFN2 in LPS-induced microglia in response to treatment with TEPP-46 10 μM, 12 h (**A**) and shikonin 10 μM, 30 min (**B**) following LPS 1 μM, 12 h. **C-E.** Genetic inhibition of MFN2. RT-qPCR (**C**) and Western blot analysis (**D-E**) of MFN2 expression in primary microglia after knockdown of MFN2 by PKM2-specific small interfering RNA (siPKM2(1), siPKM2(2),

siPKM2(3)) after 12 h. **F-J.** qPCR analysis of TNF-α(**F**), IL-6 (**G**), IL-1β (**H**), CD206 (**I**) and IL-10 (**J**) in LPS-induced microglia after knockdown of MFN2 and TEPP-46 (10 μM, 12 h) treatment. **K-L.** Analysis of the mitochondrial membrane potential (mtΔΨ) in primary microglia as indicated treatment. **K.** Representative images showing flow cytometry analysis of JC-1 staining. **L.** Statistical analysis of the JC-1 aggregate ratio (red/green). Sample size: n=3/group for Co-IP, n=3-4/group for qPCR, n=3/group for flow cytometry analysis. The data are presented as the means ± SD; **P* < 0.05, ***P* < 0.01, ****P*< 0.001vs control group. #P < 0.05, ##P < 0.01 vs LPS group.

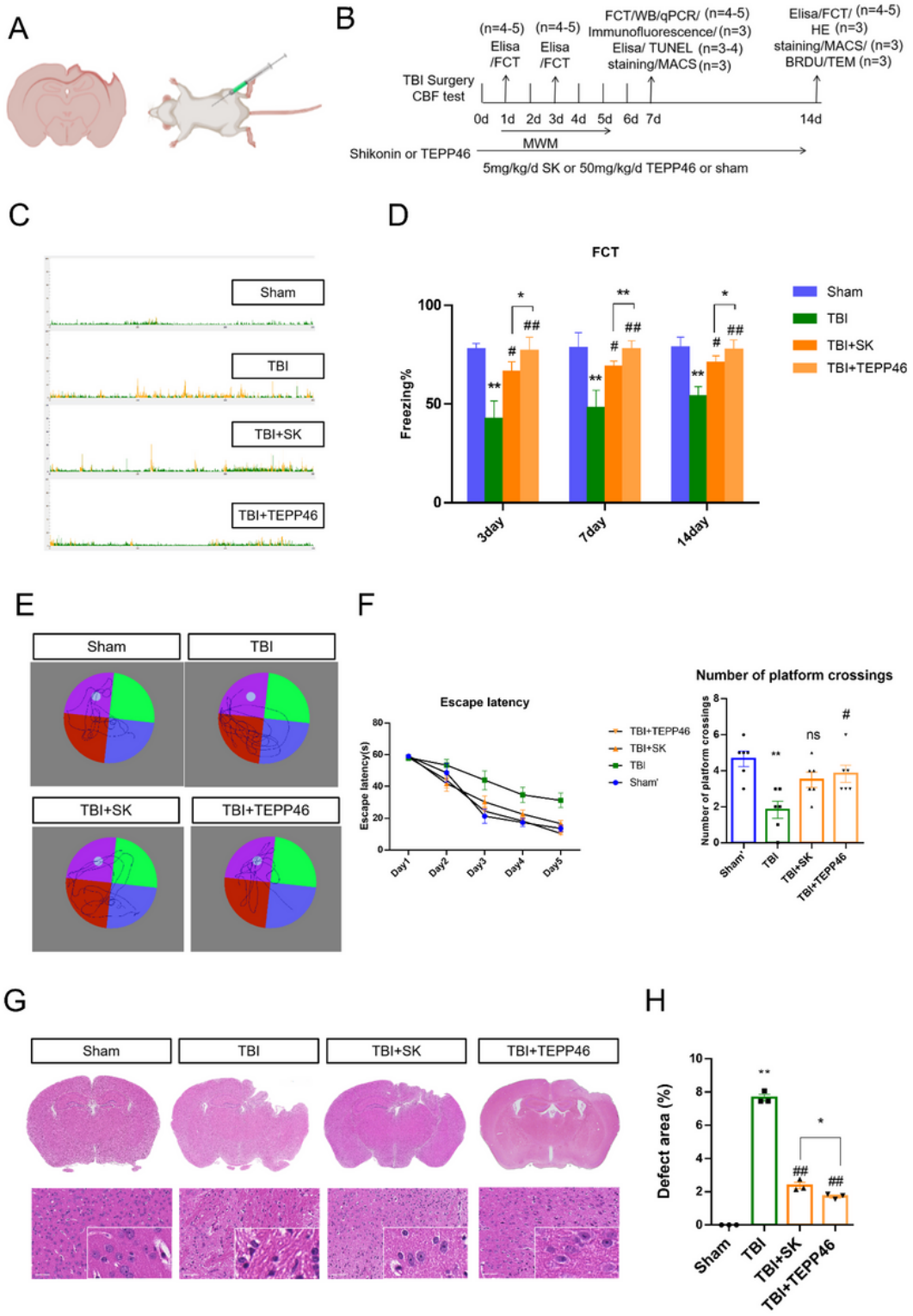

Figure 6

Tetramerization of PKM2 in microglia alleviate cognitive impairment following traumatic brain injury. **A.** The schematics of brain injury caused by controlled cortical impact (CCI) animal model and route of administration via intraperitoneal injection. **B.** The treatment scheme and timeline of behavioral and biochemical analysis. **C-D.** Contextual fear conditioning at 3-, 7- and 14-days post-injury. **E-F.** Morris water maze test at 14-days post-injury**. G-H. (G)** First line: tissue loss after TBI detected using coronal hematoxylin and eosin (HE) staining and the macro brain photographed, second line: enlarged image of lymphocytic infiltration. **(H)** The quantitative analysis of brain injury area. Scale bar=100 μm. Sample size: n=5/group for morris water maze test; n=5/group for fear conditioning test, n=3/group for HE staining. The data are presented as the means ± SD; $*P < 0.05$, $**P < 0.01$vs Sham group. $^{\#}P < 0.05$, $^{\#\#}P < 0.01$vs TBI group.

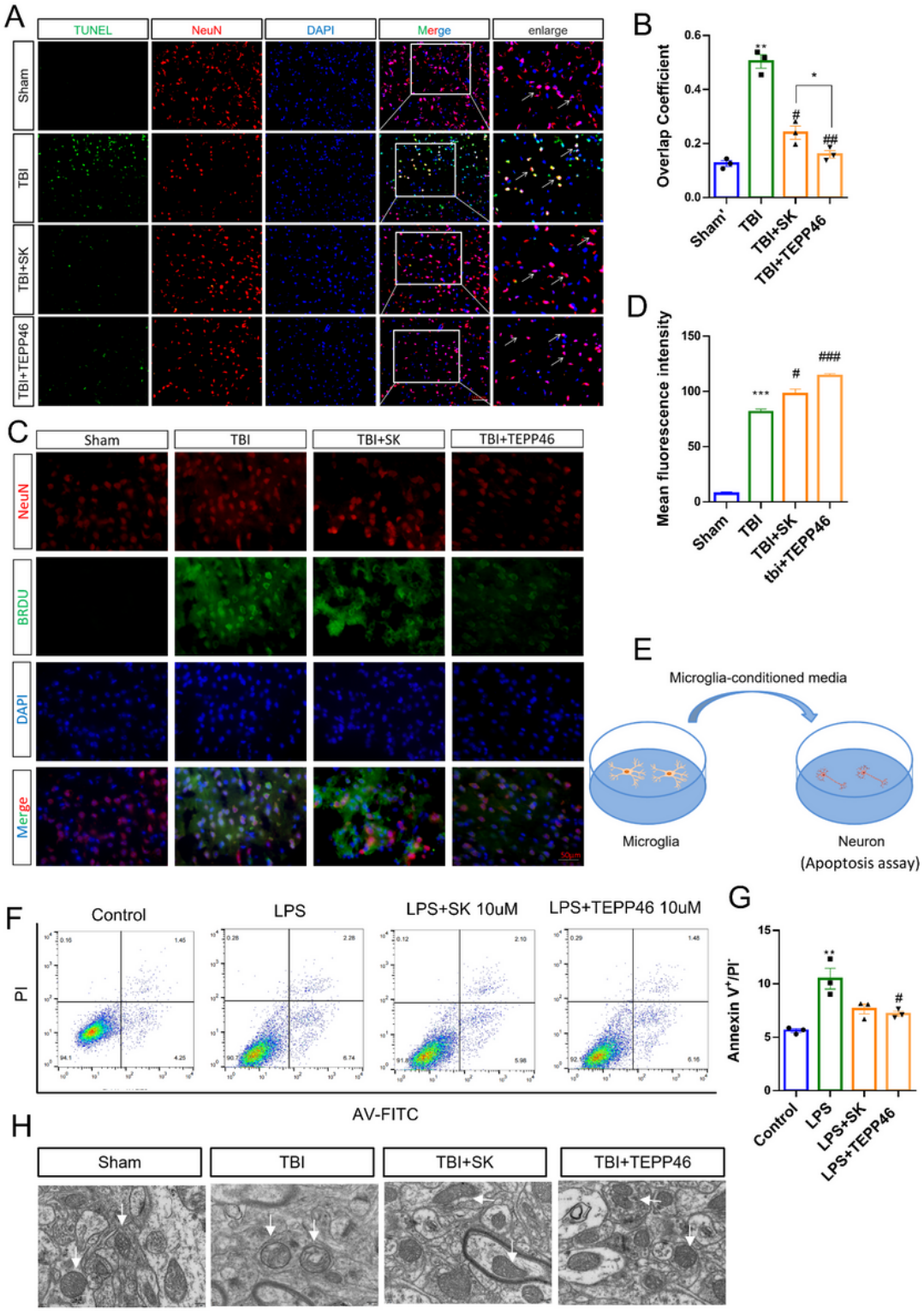

Figure 7

Tetramerization of PKM2 in microglia increased neurogenesisand neurons survival following TBI. **A-B** Representative photographs of TUNUL staining and the quantitative analysis of TUNUL-positive Neurons 14 days post-injury, Scale bar=100 μm.**C-D.** Representative images of BrdU (red), and NeuN (green) and quantifcation of percentage of BrdU-positive Neurons. **E.** Representative photomicrographs of N2a mouse neuroblastoma cell treated with conditioned media from activated BV2 microglia. **F.** Representative

images showing flow cytometry analysis of the Annexin-FITC/PI staining of neurons treated with differently conditioned media from activated BV2 microglia treated by shikonin or TEPP-46 as indicated. **G** Statistical analysis of the percentage of living cells corresponding to left panel (Apoptosis - cells). **H**. Representative TEM images of mitochondrial morphology followingTBI with TEPP-46 treatment, Scale bar=200nm. Sample size: n=3/group for TUNULstaining, n=3/group for BrdU staining, n=3/group for TEM analysis. The data are presented as the means ± SD; *P < 0.05, **P < 0.01vs Sham group. #P < 0.05, ##P < 0.01vs TBI group.

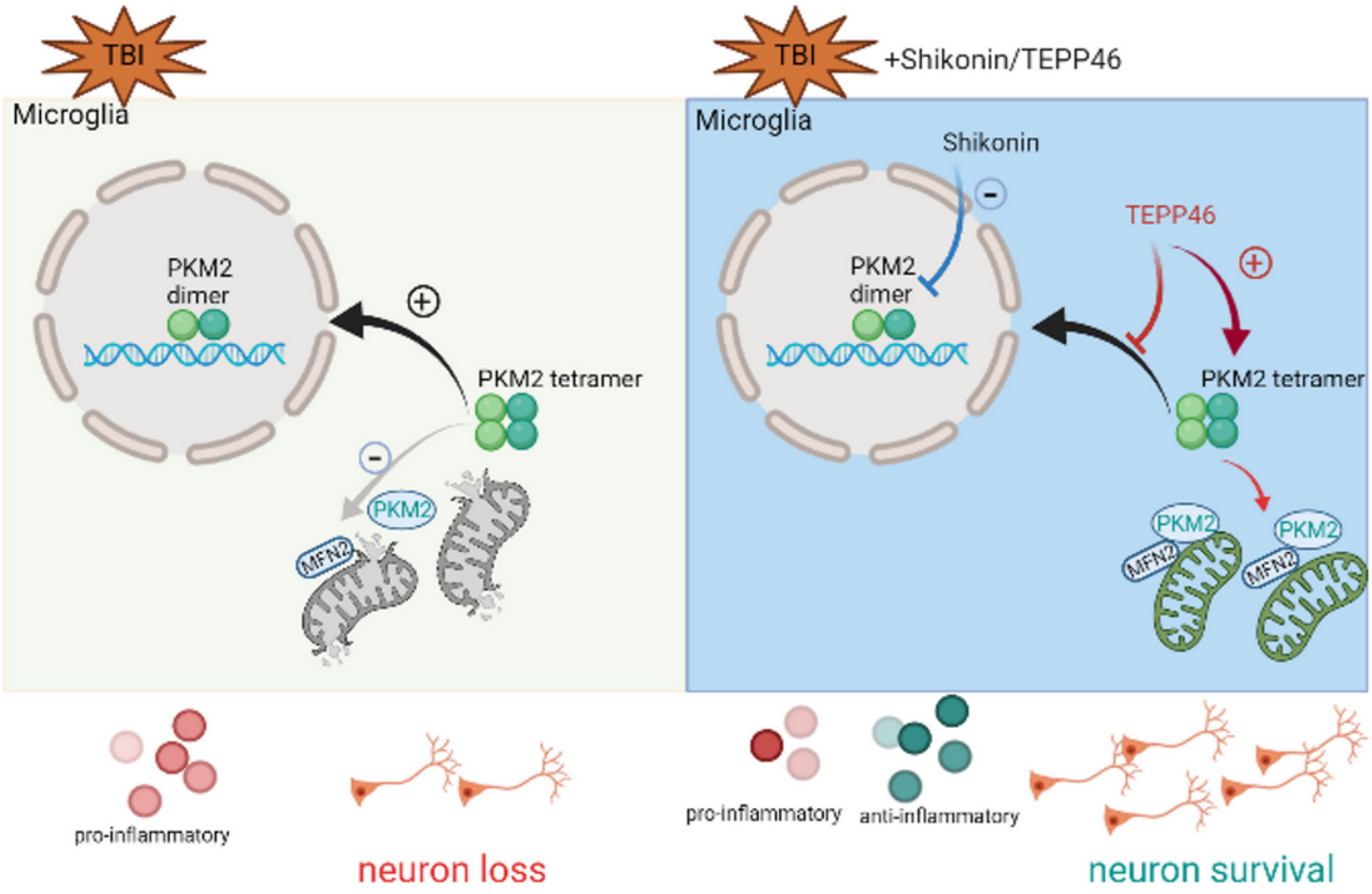

Figure 8

During the acute and subacute phases of TBI, dimeric PKM2 is stimulated and translocate to the nucleus to interact with transcript factors, leading to the production of pro-inflammatory cytokines and M1 microglia polarization. Shikonin significantly reduced the expression levels of both PKM2 dimers and tetramers, whereas TEPP-46 treatment resulted in a significant increase in tetrameric PKM2 and enhanced the interaction between PKM2 and MFN2 in primary microglia, which plays a partial role in the regulation of microglial phenotypic transitions. Ultimately, TEPP-46 exhibited a better treatment effect on neuronal loss and cognitive impairment following TBI, compared to the inhibition of total PKM2 in microglia by shikonin.

Supplementary Files

This is a list of supplementary files associated with this preprint. Click to download.

- SupplementaryInformation.pdf